Selective inhibition of parallel DNA damage response pathways optimises radiosensitisation of glioblastoma stem-like cells

Running title: Radiosensitisation of glioblastoma stem-like cells

Shafiq U Ahmed[1, 4], Ross Carruthers[1], Lesley Gilmour[1], Salih Yildirim[2], Colin Watts[3] and Anthony J Chalmers[1, 4]

Author affiliations:

[1]Translational Radiation Biology, Institute of Cancer Sciences, Wolfson Wohl Cancer Research Centre, University of Glasgow, Glasgow, G61 1QH, UK.

[2] Present address: Muhendislik Fakültesi, Karabuk Universitesi, Karabuk, Turkey

[3]Department of Clinical Neurosciences, Division of Neurosurgery, ED Adrian Building, Forvie Site, Robinson Way, Cambridge University, Cambridge, CB2 0PY, UK.

[4]Corresponding authors

Financial support:
Financial support for this study was provided by Medical Research Council (MRC) grant to Anthony J Chalmers

Author contact details
Shafiq U Ahmed: Shafiq.Ahmed@glasgow.ac.uk, (Telephone: 0141 330 3984)
Ross Carruthers: Ross.carruthers@glasgow.ac.uk
Lesley Gilmour: Lesley.Gilmour@glasgow.ac.uk
Salih Yildirim: salihyildirim@karabuk.edu.tr
Colin Watts: cw209@cam.ac.uk
Anthony J Chalmers: Anthony.chalmers@glasgow.ac.uk, (Telephone: 0141 330 6426)

Author Contributions
Conception and Design: Shafiq U Ahmed, Ross Carruthers, Anthony J Chalmers
Development of methodology: Shafiq U Ahmed, Ross Carruthers, Lesley Gilmour, Salih Yildirim
Acquisition of data: Shafiq U Ahmed, Ross Carruthers, Lesley Gilmour
Analysis of data: Shafiq U Ahmed, Ross Carruthers, Lesley Gilmour
Writing/review of manuscript: Shafiq U Ahmed, Colin Watts, Anthony J Chalmers
Study supervision: Anthony J Chalmers

Potential conflicts of interest: None

Key Words: Glioblastoma stem-like cells, DNA damage response (DDR), DDR inhibitors, ionising radiation, radiosensitisation

Word count: 5749 (Introduction/Materials and methods/Results/Discussion)

Abstract

Glioblastoma (GBM) is the most common form of primary brain tumour in adults and is essentially incurable. Despite aggressive treatment regimens centred on radiotherapy, tumour recurrence is inevitable and is thought to be driven by GBM stem-like cells (GSCs) that are highly radioresistant. DNA damage response pathways are key determinants of radiosensitivity but the extent to which these overlapping and parallel signalling components contribute to GSC radioresistance is unclear. Using a panel of primary patient-derived GBM cell lines, we confirmed by clonogenic survival assays that GSCs were significantly more radioresistant than paired tumour bulk populations. DNA damage response targets ATM, ATR, CHK1 and PARP-1 were upregulated in GSCs and CHK1 was preferentially activated following IR. Consequently, GSC exhibit rapid G2/M cell cycle checkpoint activation and enhanced DNA repair. Inhibition of CHK1 or ATR successfully abrogated G2/M checkpoint function, leading to increased mitotic catastrophe and a modest increase in radiation sensitivity. Inhibition of ATM had dual effects on cell cycle checkpoint regulation and DNA repair that were associated with greater radiosensitising effects on GSCs than inhibition of CHK1, ATR or PARP alone. Combined inhibition of PARP and ATR resulted in a profound radiosensitisation of GSCs which was of greater magnitude than in bulk populations and also exceeded the effect of ATM inhibition. These data demonstrate that multiple, parallel DNA damage signalling pathways contribute to GSC radioresistance and that combined inhibition of cell cycle checkpoint and DNA repair targets provides the most effective means of overcome radioresistance of GSC.

Word count: 247

Introduction

Glioblastoma (GBM) is the most common primary brain tumour in adults. Despite optimal treatment consisting of surgical resection followed by radiotherapy with concomitant and adjuvant temozolomide chemotherapy, median survival remains dismal at 12–15 months (1). Responses to treatments are inevitably followed by relapse, typically within the maximally irradiated volume (2,3). In GBM tumourigenic cells display complex clonal dynamics in which genetically distinct sub-clones have variable serial repopulating activity *in vivo* (4,5). Such a functional readout is likely to represent activity of self-renewing GBM 'stem-like' cells (GSCs) whose competitive self-renewal ability varies on the basis of frequency and/or quantitative features and underpins the evolution of resistant disease (6). Consistent with this GSCs that express stem cell markers such as CD133, SSEA-1 (CD15), Nestin, SOX2 and Olig2 (7-10) are more resistant to radiotherapy and conventional chemotherapy than more differentiated epigenetically stable 'tumour bulk' cells (10-14). Thus there is an urgent need to develop targeted treatment strategies that will overcome the innate resistance of GSCs, improve local tumour control and extend patient survival.

Radiotherapy is a vital therapeutic modality for GBM which at a cellular level causes single and double stranded DNA breaks that evoke a multifaceted DNA damage response (DDR). At the apex of the DDR lie the serine/threonine protein kinases ataxia telangiectasia mutated (ATM) and ataxia telangiectasia and Rad3-related (ATR) which maintain genomic integrity by activating cell cycle checkpoints and DNA repair pathways (15). ATM is mainly activated by DNA double-strand breaks (DSBs) whereas ATR responds to single-stranded regions of DNA generated at stalled replication forks and during processing of DSBs by nucleases (16-19). The MRN (MRE11-RAD50-NBS1) complex has key roles in sensing and processing DSBs as well as activating ATM and ATR (20). ATR activates cell cycle checkpoint kinase proteins including CHK1 whereas ATM functions primarily through activation of CHK2. These downstream checkpoint kinases activate G1 and G2/M cell cycle checkpoints through phosphorylation of phosphatases CDC25A, CDC25C and kinases CDK1 and Wee1 that regulate cell cycle progression (21). Additionally, ATM promotes repair of a subset of DSBs. Poly(ADP-ribose) polymerase (PARP) facilitates repair of radiation induced single strand breaks (SSBs) and the radiosensitising effects of PARP inhibitors are well characterised (22). This brief summary illustrates key components of the complex network of overlapping and parallel DDR pathways that dictates cellular outcomes after radiation treatment.

There is growing evidence that DDR signalling is upregulated in GBM and integral to GSC radioresistance. Analysis of GBM clinical samples has revealed high levels of p-ATM, p-CHK1, p-CHK2 and PARP1 compared to normal brain tissue (23,24). Furthermore, basal levels of p-CHK1, p-CHK2 and Rad17 have been shown to be higher in CD133+ GSCs compared to non-tumourigenic CD133- populations, a finding that was associated with radioresistance of the GSC population (10). However, subsequent studies have either failed to show differences in DNA repair capacity based on CD133 status or revealed increased radiosensitivity of CD133+ GSCs compared to established GBM cell lines (25,26). Such discrepancies may reflect methodological differences or comparisons between non-isogenic cell lines. Indeed, we have recently demonstrated that radioresistance of GSC populations is associated with enhanced ATM dependent DSB repair proficiency (27).

Currently there is intense research into the development of small molecule inhibitors of DDR proteins (DDRi), one aim of which is to increase the therapeutic index of standard treatments (28). This is driven by several factors: (i) DNA is the major target for many anticancer therapies, (ii) constitutive activation of DDR is frequently observed in cancers (29) and (iii) activation of DDR is associated with resistance to cytotoxic therapies. Several preclinical studies have successfully utilised DDRi to increase chemo- and radiosensitivity in GBM models but these results were not substantiated in the treatment resistant GSC population (30-34). More recently we have shown the ATM inhibitor KU55933 to be a potent radiosensitiser of GSC (27) and inhibition of PARP has also been shown to overcome radioresistance of GSCs (35). These findings corroborate and extend the landmark study by Bao and colleagues in which inhibition of CHK1 and CHK2 using debromohymenialdisine was shown to enhance the radiosensitivity of GSCs (10).

The observation that GSCs exhibit upregulated DDR signalling provides both opportunities and challenges. Whilst targeting individual components of this complex network can increase the radiosensitivity of GSC, the relative contributions of these components and the implications of multiple DDR pathways and mechanisms contributing to radioresistance remain unexplored. We addressed this by utilising paired, primary, patient derived GBM cell lines cultured to enrich for or deplete the GSC population ('GSC' and 'bulk' populations respectively). We show that GSCs express higher total and activated levels of DDR targets than bulk populations and that this phenotype is maintained in orthotopic xenograft models and GBM patient specimens. Our mechanistic studies highlight rapid activation of cell cycle checkpoint and enhanced DNA repair as key determinants of GSC radioresistance. We show that, although selective inhibition of either pathway increases radiosensitivity of GSC, effects are limited by reciprocity between these signalling conduits. Accordingly, combined inhibition of ATR and PARP1 significantly enhanced the radiosensitivity of GSCs, and the magnitude of this effect was greater than in bulk populations. We propose that targeting of parallel DDR pathways is required to maximise radiosensitisation of GSCs and optimise outcomes for GBM patients.

Word count: 867

Materials and Methods

Derivation and maintenance of primary and patient derived GBM cell lines

Primary patient derived GBM cell lines E2, G7, R10, R15 and R24 were derived from freshly resected tumour specimens and maintained as described previously (22,36). Patient consent was sought before surgery and tissue collection was approved by the local regional Ethics Committee (LREC ref 04/Q0108/60) and compliant with the UK Human Tissue Act 2004 (HTA Licence ref 12315). Each cell line was cultured in pairs either on Matrigel™ (Life Technology) coated flasks in AdvDMEM F12 medium (Gibco) supplemented with 1% B27 (Invitrogen), 0.5% N2 (Invitrogen), 4µg/ml heparin, 20ng/ml bFG, 20ng/ml EGF (Sigma), and 1% L-Glutamine to maintain the GSC population or in MEM (Gibco) supplemented with 10% FBS Sigma, 1% L-glutamine and 1% sodium pyruvate to deplete the GSCs and generate a differentiated tumour bulk population. All cell cultures were maintained at 37^0C, 5% CO_2. Cell lines were utilised between 6-15 passages and then discarded.

Generation of orthotopic tumours and immunohistochemistry

Tumours were generated by injecting 1 x 10^5 cells in CD1 nude mice as described previously (37), and in supplementary materials and methods. Immunohistochemistry was performed on paraffin embedded sections. Following antigen retrieval sections were incubated with anti-Ki67, PARP-1 or p-ATM antibodies overnight followed by incubation with secondary antibodies. Staining was visualised by application of DAB.

Drug treatment and radiation

ATM inhibitor KU-55933 (Tocris bioscience), ATR inhibitor VE821, PARP inhibitor olaparib, CHK1 inhibitors SCH900776 and CHIR-124 (Selleckchem), hydroxyurea and aphidicolin (Sigma) were all dissolved in DMSO. For drug-radiation combination studies, cells were exposed to fresh media containing the inhibitor or relative DMSO control for 1 hour prior to irradiation in tissue culture vessels using an XStrahl RS225 cabinet at room temperature with 195kV/15mA X rays producing a dose rate of 1.6 Gray per minute. For UV studies, media containing the drug was removed after one hour and cells were irradiated using a UV Stratalinker (Stratagene).

Clonogenic and neurosphere assays

Paired GSC and bulk population from E2 and G7 cell lines formed countable colonies and were seeded at a density of 250 cells per well in Matrigel coated 6 well dishes for 24 hours. Wells were treated with the inhibitors or relative DMSO control for 1 hour followed by mock or 1-5Gy irradiation. Cells were then incubated for a further 24 hours followed by replacement with fresh media. E2 and G7 colonies were fixed after 2 or 3 weeks respectively in methanol followed by staining with crystal violet. Colonies consisting of minimum 50 cells were counted manually and using an automated colony counter (GelCount™, Oxford Optronix). Clonogenic survival data were fitted using a linear quadratic model and $SER_{0.37}$ and SF_{4Gy} values were calculated from the fitted curve. ANOVA test was used to analyse differences between clonogenic survival curves.

For neurosphere assay 10 GSCs were seeded into each well of a 96 well plate in 100µL medium containing the drug or relative DMSO control for 1 hour followed by mock or 2Gy irradiation. 48 hours later a further 150 µL of fresh media was added per well. Neurospheres were manually counted under 5x magnification after 3 or 4 weeks for G7 and E2 GSC respectively.

Immunofluorescence

Paired bulk and/or GSCs were plated on coverslips coated with Matrigel and treated with radiation alone or in combination with the inhibitors for 24 hours. Cells were fixed and incubated with γ-H2AX or p-His H3 S10 antibodies overnight at 4^{o}C followed by incubation with secondary conjugated antibodies. Nuclei were counterstained with Vectashield containing DAPI. Images were acquired using Zeiss LSM 710 confocal microscope and analysed using Velocity software (PerkinElmer). γ-H2AX foci data are presented as box and whisker plots from 3 independent experiments unless otherwise stated and analysed using Mann Whitney U-test as they were not normally distributed.

Flow cytometry, cell cycle distribution and proliferation and cell death

For analysis of mitotic population, cells were treated and fixed with 70% ethanol and incubated with p-His H3 S10 antibody followed by γ-H2AX antibody and analysed using flow cytometry. Combined annexin V and PI analysis was carried out according to manufacturer's protocol (BD Biosciences). Analysis of GSC markers was carried out using conjugated CD133 and CD15 (Miltenyi Biotech). FACS was carried out using FACSAria Fusion following labelling with CD133/CD15-PE conjugated antibodies (Miltenyi Biotech). Live cells were gated and sorted populations were plated into 6 well plates in identical stem cell culture media for 3-7 days before harvesting. Cell cycle distribution was determined following 40 minutes incubation with 10µM BrdU followed by flow cytometric analysis according to manufacturer's protocol (BD Biosciences). Data was analysed using FlowJo software (Tristar). Analysis of caspase 3/7 activity was carried out using Caspase-Glo 3/7 kit (Promega).

Cell proliferation was measured in 96 well plates with 200-400 cells seeded per well in replicates of 5. Every 24-48 hours plates were fixed in 4% formaldehyde followed by DAPI staining. Nuclei were counted using Operetta (PerkinElmer). Cell doubling times were calculated from exponential growth curve fits using GraphPad Prism.

Western blotting

For immunoblotting whole cell lysates were prepared and processed in SDS buffer, blotted onto membranes and probed with primary antibodies (supplementary material and methods) overnight followed by appropriate secondary antibodies for 1-3 hours. Bound antibodies were visualised using chemiluminescence (Thermo Scientific) and bands quantified using Image J.

Statistical Analyses

All experiments were repeated 3 times unless otherwise stated and data points reported as mean +/- SEM. Statistical analysis and graphs were produced using Minitab 16 and Graphpad Prism 6. Unpaired t-test or one sample t-test were used to generate *p* values.

Word count: 918

Results

GSC populations are radioresistant

We have previously characterised two primary GBM cell lines (E2 and G7) (27,37). Using the same techniques three additional primary GBM cell lines (R10, R15 and R24) were expanded by culturing under selective media to enrich for or deplete the GSC population. We demonstrated that GSC enriched populations of E2, G7 (27,37), R10 and R15 cells generate orthotopic tumours in immunodeficient mice that recapitulate the human disease, whereas GSC depleted, tumour bulk populations do not (supplementary Figure S1). While the neural stem cell markers nestin, SOX2, CD133, Olig2 and CD15 were heterogeneously expressed between different GSC cultures, expression of these markers was consistently increased in GSCs compared to bulk populations (Figure 1A and 1B). Clonogenic survival assays in E2 and G7 cell lines confirmed GSC cultures to be more radioresistant than paired bulk populations. Dose modifying factors calculated at 37% survival ($DMF_{0.37}$) showed that E2 and G7 GSCs were more radioresistant than corresponding bulk populations by factors of 1.36 ($p=0.001$) and 1.44 ($p<0.001$) respectively (Figure 1C-E). Radioresistance of GSC populations was confirmed by comparing surviving fraction at 4Gy (SF_{4Gy}, supplementary Table 1). These findings were consistent with the observation that E2 and G7 GSCs were refractory to cell death as measured by Annexin-V and propidium iodide staining following treatment with high radiation doses (15 and 30 Gy, Figure 1F, supplementary Figure S2). Caspase 3/7 activity assays supported the assertion that GSC populations are extremely resistant to radiation induced apoptotic cell death (Figure 1G).

GSCs express high levels of DDR targets under basal conditions and activate CHK1 rapidly following IR

DDR targets have previously been shown to be upregulated and associated with GSC radioresistance (10,27,35). We explored this further in our GSC and bulk culture models and observed an overall pattern of higher levels of total and phosphorylated CHK1 (S345) and ATR (S428) in GSCs compared to bulk populations in primary GBM cell lines (Figure 2A). Importantly this was not an artefact of culture conditions since CD133 or CD15 positive sorted cells exhibited significantly higher levels of phosphorylated CHK1 than negative sorted populations of E2, R24 and G7 cell lines cultured in the same conditions (Figure 2B). Higher levels of total CHK1 were also observed in R24 and G7 cells expressing the relevant stem cell marker.

We next explored if differences in cell cycle distribution could account for the disparate CHK1 levels observed in GSC and bulk populations since CHK1 is typically expressed in S and G2 phases of proliferating cells. Analysis of BrdU incorporation indeed revealed significant differences in cell cycle profiles between these two populations (Figure 2C and supplementary Figure S3) with GSCs exhibiting a marked increase in the percentage of cells in S and G2 phases of the cell cycle. Interestingly, the differences in cell cycle distribution had no significant impact on cell doubling times, which were similar in GSC and bulk populations in both E2 and G7 cell lines (supplementary Figure S3). While these results might explain the observed increase in CHK1 levels in GSC they also indicate that enhanced radioresistance of GSCs is not a consequence of reduced proliferation rates.

Further interrogation of DDR markers revealed higher levels of PARP-1 and phosphorylated ATM (p-ATM, S1981) in the majority of the GSC populations (Figure 2A). To confirm these findings *in vivo* we generated xenograft tumours from E2 and G7 GSC using an orthotopic mouse model. Analysis of tumour sections revealed a heterogeneous pattern of p-ATM (S1981) and PARP-1 staining highlighting differential protein expression between different cell populations (Figure 2D). PARP-1 staining in G7 tumours was abundant and homogeneous, consistent with previous reports proposing PARP-1 as a GBM marker (24). These findings were reproduced in a clinical GBM specimen, which exhibited marked p-ATM and PARP-1 expression in the majority of tumour cells (Figure 2D). These data illustrate collective upregulation and/or activation of DDR targets in GSC populations under basal conditions *in vitro* and in a subpopulation of GBM cells *in vivo*.

We next sought to investigate how differences in basal CHK1 levels between GSC and bulk populations affect the DDR. Irradiation of E2 GSCs evoked more pronounced activation of CHK1 than in the corresponding bulk populations as demonstrated by a significantly greater increase in the phospho-CHK1 S345: total CHK1 ratio within 15 minutes that was maintained for at least 3 hours (Figure 2E and 2F). Reduced CHK1 activation in E2 bulk cells occurred despite similar levels of DNA damage induction (γ-H2AX). While the relative extent of radiation induced CHK1 activation was similar in bulk and GSC populations of G7 cells (supplementary Figure S4), absolute levels of CHK1 and p-CHK1 were significantly higher in G7 GSC than in paired bulk cells both under basal conditions and following irradiation. CHK2 activation (T68 phosphorylation) was similar in E2 GSC and bulk populations although differences were observed between G7 bulk and GSC populations (Figure 2E and supplementary Figure S4). We explored the possibility that enhanced activation of CHK1 in GSC could be caused by 'priming' of the MRN (MRE11, RAD50, NBS1) DNA damage sensor complex under basal conditions. No differences in total or phosphorylated MRE11 and NBS1 between GSC and bulk populations were observed under basal conditions or following irradiation, but modest upregulation of RAD50 was observed in E2 and G7 GSCs following irradiation (Figure 2E, supplementary Figure S4). The possibility that CHK1 activation was delayed (rather than reduced) in bulk cells was excluded by demonstrating that S296 phosphorylation of CHK1 was attenuated in E2 and absent in G7 bulk cells but maintained in both GSC cultures at 6, 12 and 24 hours after irradiation (Figure 2G). While some variation in the kinetics of CHK1 activation in GSCs was observed between different experiments, which could be due to the use of different batches of frozen primary patient derived cells, both phosphorylated and total CHK1 levels were consistently higher in GSCs than bulk cells and were reproducibly augmented at all time points following radiation. Finally, the enhanced CHK1 activation in GSC was not only a radiation specific phenomenon: E2 and G7 GSC also exhibited markedly enhanced activation of CHK1 (S345 and S296 phosphorylation) in response to UV, hydroxyurea or aphidicolin treatments despite levels of γ-H2AX induction that were comparable to bulk populations (Figure 2H, supplementary Figure S4).

Rapid induction of CHK1 in GSCs is associated with enhanced G2/M cell cycle checkpoint activation

We next investigated the impact of enhanced CHK1 activation on cell cycle checkpoint responses of GSCs. Both E2 and G7 cell lines were refractory to radiation induced G1/S

checkpoint activation, consistent with frequent deregulation of p53 signalling pathways in GBM (38) (supplementary Figure S5). However, analysis of the G2/M checkpoint by flow cytometric quantification of mitotic cells identified by S10 phosphorylation on histone H3 (p-His H3) revealed that GSC activated G2 arrest significantly more efficiently than paired bulk populations, requiring less time to reduce the mitotic cell population by 50% following IR treatment (Figure 3A, supplementary Figure S6). Consistent with this, E2 CD133+ sorted cells activated G2 arrest more rapidly and completely than CD133- cells cultured in the same conditions (supplementary Figure S7). Intriguingly, E2 bulk cells failed to fully activate the G2/M checkpoint at any time point (Figure 3C). Further dose response studies revealed that depletion of mitotic cell fraction by 75% occurred after significantly lower radiation doses in E2 and G7 GSC compared to bulk populations (Figure 3B, supplementary Figure S6) and that E2 and G7 bulk cells were released from the G2/M checkpoint earlier than GSC (Figure 3C). Taken together our results indicate that increased and/or more rapid activation of CHK1 might be responsible for the enhanced radioresistance of GSC and that the relative radiosensitivity of tumour bulk cells (Figure 1) might be at least partly explained by these cells entering mitosis carrying unrepaired DNA damage (see also Figure 6).

Radiosensitising effects of CHK1 inhibition are more pronounced in GBM bulk cells than GSCs

Reasoning that radioresistance of GSCs might be driven by enhanced CHK1 mediated activation of the G2/M checkpoint, we hypothesised that inhibition of CHK1 would abrogate the G2/M checkpoint and increase radiosensitivity. To investigated this we utilised SCH 900776 (SCH) a well characterised CHK1 specific inhibitor which had no significant effect on CHK2 activity as highlighted by unaltered phosphorylation of T68 (Figure 4A-C) (39,40). As expected, SCH treatment alone inhibited CHK1 S296 autophosphorylation in a dose dependent manner and induced CHK1 S345 phosphorylation through CHK1 dependent inhibition of the PP2A phosphatase feedback loop (41) (Figure 4A and 4C, supplementary Figure S8). Treatment of E2 GSCs with SCH resulted in enhanced induction of CHK1 S345 phosphorylation by UV or IR along with increased γ-H2AX levels reflecting increased DNA damaging signalling in response to CHK1 inhibition (Figure 4A-C and supplementary Figure S8). Interestingly, induction of CHK2 T68 phosphorylation was also observed following combined treatment with SCH plus IR suggesting compensatory activation of CHK2 following CHK1 inhibition (Figure 4C) (42). In addition SCH treatment alone generated a γ-H2AX signal highlighting a basal function of CHK1 in maintaining genomic stability (43). Additional biomarkers of CHK1 inhibition included downregulation of phosphorylated Wee1 (S642) and CDC25C (T48) whilst upregulation of CDC25A was observed following SCH treatment alone and augmented in combination with radiation, consistent with enhanced cell cycle progression despite the presence of damaged DNA (Figure 4B and 4C, supplementary Figure S8).

Since our earlier results showed that GSCs rapidly activate the G2/M cell cycle checkpoint in response to IR (Figure 3), we hypothesised that CHK1 inhibition would abolish this effect and thus overcome the radioresistant GSC phenotype. Indeed, SCH treatment abrogated radiation induced G2 arrest in E2 and significantly attenuated it in G7 GSCs, while SCH treatment in the absence of radiation was sufficient to drive E2 and G7 GSCs into mitosis (Figure 4D). Importantly, clonogenic survival assays confirmed significant radiosensitisation

of E2 and G7 GSC by CHK1 inhibition as illustrated by sensitisation enhancement ratios at 37% survival ($SER_{0.37}$) of 1.9 and significant reductions in surviving fractions at 4Gy (SF_{4Gy}) in both cell lines (Figure 4E and 4F). Despite the limited ability of bulk populations to phosphorylate CHK1 and induce G2/M checkpoint activation in response to radiation, a similar or greater magnitude of radiosensitisation ($SER_{0.37}$=2.3-2.4) was observed in bulk populations treated with SCH. This unexpected observation was confirmed using an alternative CHK1 inhibitor CHIR-124 (44) (supplementary Figure S9). While these data support the assertion that CHK1 inhibition has therapeutic potential in GBM, the observation that overexpression and constitutive activation of CHK1 in GSCs was not associated with increased radiosensitisation by CHK1 inhibitors indicates that additional mechanisms could be responsible for limiting the radiosensitisation effects of CHK1 inhibition in the GSC population.

Inhibition of CHK1 radiosensitises GSC through a mechanism involving mitotic catastrophe

Our subsequent studies were aimed at investigating the mechanisms responsible for (i) GSC radiosensitisation by CHK1 inhibition and (ii) enhanced radiosensitisation of bulk cells. Initial analysis of DNA damage in E2 GSCs using flow cytometry highlighted a significant increase in the γ-H2AX positive cell population following combined SCH and IR treatment compared to individual treatments alone (Figure 5A and 5B). Interestingly, SCH treatment alone induced a γ-H2AX response, confirming our earlier observations (Figure 4A-C). Since this signal was observed predominantly in S-phase cells, we inferred that CHK1 inhibition exacerbates replication stress in GSCs. Since SCH treatment also inhibited the G2/M checkpoint (Figure 4D) we investigated whether treated GSCs would enter mitosis with damaged DNA. Indeed, following SCH treatment we observed a distinct population of mitotic cells with high γ-H2AX signal that was significantly increased after combined treatment with SCH and IR (Figure 5C and 5D). Immunofluorescence analysis confirmed these results, demonstrating a distinct mitotic cell population with intense, pan-nuclear γ-H2AX staining (middle row, Figure 5E). This is likely to represent cells in the initial stages of mitotic catastrophe, which was clearly visible in a separate population of mitotic cells characterised by loss of membrane integrity and fragmented morphology (bottom row). Both populations were augmented in GSCs following combined treatment with SCH and IR relative to either treatment alone. In addition, we evaluated the consequence of mitotic division in cells with damaged DNA and found a significant increase in the percentage of GSCs harbouring one or more micronucleus following the combined treatment (Figure 5F). Taken together, our data demonstrate that CHK1 inhibition sensitises GSC to IR by preventing G2/M checkpoint activation, allowing mitotic entry of cells bearing damaged DNA resulting in mitotic catastrophe and genomic instability.

Limited radiosensitisation of GSCs by CHK1 inhibition is explained by enhanced DNA repair

We next sought to identify the mechanism responsible for limiting the radiosensitising effects of CHK1 inhibition in GSCs by comparing effects of IR plus SCH with those observed in paired bulk cell populations in which SCH had shown more pronounced radiosensitising effects (Figure 4E and 4F). Analysis of G7 cells revealed a significant increase in both total and mitosis specific γ-H2AX positive cells in the bulk population compared to GSCs following

treatment with SCH alone or in combination with radiation (Figure 6A and 6B). Similarly, significantly more mitotic catastrophe events were observed in bulk populations than in GSCs (Figure 6C). Although E2 GSCs treated with SCH and IR showed an increased total number of γ-H2AX positive cells compared to the paired bulk cells, this did not translate into increased mitotic damage or mitotic catastrophe (supplementary Figure S10). Indeed, even when SCH and IR had increased the DNA damage burden in E2 GSCs, the majority of these cells proceeded to mitosis having repaired this damage, as indicated by a significant reduction in γ-H2AX positive mitotic cells and fewer cells exhibiting mitotic catastrophe compared to the paired bulks population (Supplementary Figure S10). Thus, enhanced DNA repair appears to compensate for the significant increase in DNA damage observed in GSCs treated with radiation and CHK1 inhibitor. Consistent with this, analysis of micronuclei, which are formed as a direct consequence of mitotic division in cells with unrepaired DNA DSBs, revealed that GSCs exhibit significantly enhanced DNA repair capacity when compared with bulk cells in both E2 and G7 cell lines (Figure 6D and supplementary Figure S10). This theory is also corroborated by the observation that a significantly higher percentage of bulk cells than GSCs harbour micronuclei under basal conditions. To substantiate this hypothesis, detailed analysis of DNA DSB repair was conducted by quantification of γ-H2AX foci in CENPF positive (G2/M) and negative (G1) cells 24 hours after high dose radiation (10 Gy). This clearly showed increased repair proficiency of GSCs compared to bulk population (Figure 6E and 6F), supporting our earlier hypothesis that enhanced DNA repair is responsible for the attenuated radiosensitising effects of CHK1 inhibition in E2 and G7 GSCs.

Optimum radiosensitisation of GSCs through parallel inhibition of DNA damage response pathways

In order to identify the optimum targets for GSC radiosensitisation we evaluated small molecule inhibitors of additional DDR proteins that were up-regulated in GSCs (Figure 2A). DNA repair was targeted using the PARP inhibitor olaparib, cell cycle checkpoints were inhibited using the ATR inhibitor VE821 and combined targeting of cell cycle checkpoints and DNA repair was evaluated using the ATM inhibitor KU55933. Results in E2 cells showed that ATR inhibition sensitised GSC and bulk populations equally although there was a trend towards increased radiosensitisation of bulk cells (Figure 7A and 7B). $SER_{0.37}$ values for ATR and CHK1 inhibition were comparable. In contrast, inhibition of PARP or ATM revealed a trend towards increased radiosensitisation of GSCs. The ATM inhibitor KU55933 proved to be the most potent radiosensitiser of GSC ($SER_{0.37}$=2.60, Figure 7B).

To understand the reasons for the different magnitudes of GSC radiosensitisation by the DDR inhibitors we investigated their effects on cell cycle checkpoints and DNA repair. Whereas inhibition of either ATR or CHK1 completely ablated radiation induced G2/M checkpoint activation (Figure 7C), inhibition of ATM had only a partial effect. In contrast, ATM inhibition significantly impaired repair of radiation induced DSBs as demonstrated by a significant increase in the number of unresolved γ-H2AX foci 24 hours post-irradiation (Figure 7D). A similar effect on DNA repair was observed following PARP inhibition. Considering that ATM inhibition was associated with the greatest radiosensitisation of GSCs we hypothesised that dual inhibition of cell cycle checkpoint activation and DNA repair might provide optimum radiopotentiation. This was investigated by concomitant inhibition of DNA

repair and cell cycle checkpoint function by combined treatment with inhibitors of PARP and ATR. As predicted, the radiosensitising effect of this combination in GSCs exceeded that of any of the inhibitors individually ($SER_{0.37}$=3.20, Figure 7E) and was significantly greater than that observed in the paired bulk cells. This is likely to be due to increased unrepaired DSBs since combined inhibition of ATR and PARP was shown to be associated with a significant increase in γ-H2AX foci in GSCs compared to the bulk population (supplementary Figure S11). To support the clinical relevance of this result we performed neurosphere formation assays using E2 GSCs and confirmed that dual inhibition of ATR and PARP achieved maximum potentiation of the inhibitory effects of radiation on neurosphere formation (Figure 7F). Taken together our results show that optimal radiosensitisation of GSCs is achieved through parallel inhibition of DDR pathways.

Word count: 2845

Discussion

GBM are heterogeneous tumours that are thought to be dependent on a cellular hierarchy that includes a privileged GSC subpopulation resistant to conventional therapy and capable of tumour propagation and growth. Uncertainty over the ideal model(s) in which to study radiation responses of the GSC population may account for the disparities in the findings of the various published studies (10,25,26). In keeping with our previous studies we generated paired cultures of primary, patient derived GBM cell lines (10,35) in which the GSC population was either enriched or depleted (27). While the use of sorted cell populations based on a specific stem cell marker such as CD133 has been questioned because both CD133+ and CD133- cells have been capable of generating tumours *in vivo* (45), we utilised this technique to validate observations made in our enriched populations and to exclude the potential confounding effects of different cell culture conditions. The GSC "signature" is likely to be complex, modulated by the cellular microenvironment and governed by multiple parameters including epigenetic and genetic aberrations which impact upon the expression of key regulatory proteins. In keeping with this interpretation, a recent publication highlights four core neurodevelopment transcription factors that are crucial to GSC maintenance and tumourigenicity (46).

Our study shows that GSCs are more radioresistant than paired bulk populations and exhibit higher expression of total and activated DDR targets under basal conditions. The reason for this is unclear; we speculate that it may reflect an endogenous response of neural stem cells to DNA damage which is subsequently maintained as part of mutagenic selection and the malignant phenotype. In addition, genetic differences between GSCs and bulk cells may affect cellular biochemistry, possibly accounting for lower proteasomal activity in GSCs contributing to higher levels of DDR targets (47). More recently increased levels of reactive oxygen species have been proposed as a mechanism responsible for upregulated PARP-1 in GSCs (35).

One surprising observation was the apparent lack of CHK1 activation in bulk cells exposed to IR. This observation and the slower DNA repair kinetics of these cells might explain why they are significantly more radiosensitive than the GSC population. Whilst our results support this, it should be emphasised that the bulk cells remain relatively radioresistant, suggesting that alternative pathways might compensate for the lack of CHK1 activation and attenuated DDR. Indeed, non-canonical DDR pathways including NOTCH, TGFβ and receptor tyrosine kinase signalling have all been associated with GBM radioresistance and may be activated in these cells (reviewed in (48). Alternatively, bulk cells may rely on DNA damage tolerance (DDT) mechanisms which utilise translesion synthesis polymerases to bypass lesions for repair at later time points (49). This provides a mechanism to tolerate DNA damage allowing cells to continue replicating and might explain the survival of bulk cells following IR despite the lack of checkpoint activation and early checkpoint release.

The MRN complex is a crucial DNA damage sensor that is recruited to and participates in DNA DSB repair. Although our results show no significant differences in the levels of total and phosphorylated components of the MRN complex between GSC and bulk populations, the rate at which the complex is recruited to damaged site and catalytic activity of specific components might conceivably be greater in GSCs thus contributing to their enhanced radioresistance.

Our study shows that multiple DDR targets including ATR, ATM, CHK1 and PARP-1 are upregulated in GSCs compared to the bulk population, and that some are also preferentially activated. Although some of these targets have overlapping functions, individually they have distinct roles which suggest that multiple DDR pathways contribute to GSC radioresistance. Our studies showed that both GSC and bulk populations were radiosensitised by CHK1 or ATR inhibition despite higher expression and activity of these proteins in GSCs. This led us to propose that alternative DDR pathways might mitigate the radiosensitising effects of CHK1 or ATR inhibition in the GSC populations. In support of this explanation, inhibition of ATM, with its dual functions in DNA repair and cell cycle checkpoint activation, yielded the most potent single agent radiosensitisation of GSCs. Importantly we confirmed this hypothesis by demonstrating that combined inhibition of ATR and PARP generated maximum radiosensitisation, and that this effect was of significantly greater magnitude in GSCs than in bulk populations. Inhibition of PARP resulted in a significant increase in DNA DSBs, which were likely to have been generated during S-phase from unrepaired DNA SSBs. In the context of ATR inhibition these cells were unable to activate the G2/M cell cycle checkpoint and thus entered mitosis carrying high levels of unresolved DSBs. We therefore propose that GSC radioresistance is driven by both enhanced cell cycle checkpoint activation and DNA repair, and that optimal radiosensitisation can only be achieved by dual inhibition of both pathways.

Our data strongly support further pre-clinical evaluation of ATR and PARP inhibitors in combination with IR as a potential treatment for GBM. This is an entirely novel approach that to our knowledge has not been investigated in any cancer models. Clearly there will be concerns over the potential *in vivo* toxicity of this combination treatment modality: ATR is essential for tissue homeostasis, highlighted by embryonic lethality of *ATR* knockout mice, whereas *PARP1* knockout in mice is less deleterious. However, clinical experience with PARP inhibitors has been extremely promising; it is tolerated well as a single agent and clinical studies in combination with radiation are progressing. To our knowledge only one clinical study is currently recruiting patients to explore ATR inhibition as a radiosensitising strategy in advanced solid tumours (www.clinicaltrials.gov). However, a pre-clinical study using the ATR inhibitor VE822 has demonstrated radiosensitisation of pancreatic tumours in mice with no apparent *in vivo* toxicity (50). The high proliferation indices of most GBM is predicted to render them more sensitive to the combination of radiotherapy, PARP inhibition (33) and ATR inhibition, and the GSC specific radiosensitisation mechanisms outlined in this paper are associated exclusively with S, G2 and M phases of the cell cycle. Since normal brain tissues are comprised almost entirely of non-replicating, post-mitotic cells with intact G1/S checkpoint and DNA repair pathways, we predict that the radiosensitising effects of the proposed combination will be exerted exclusively upon GBM tumour cells, and will have particular impact on the radioresistant GSC population.

In summary, our study provides the first detailed examination of DDR responses in GSCs and has important implications for the management of GBM. Our results support the notion that GSCs are profoundly radioresistant and identify a novel drug combination strategy targeting both cell cycle checkpoint and DNA repair functions that has potential to overcome this. Future studies will focus on *in vivo* characterisation of this strategy and will identify optimal radiation/drug combination scheduling to take forward to phase I clinical trials in GBM patients.

Word count: 1121

References

1. Stupp R, Hegi ME, Mason WP, van den Bent MJ, Taphoorn MJ, Janzer RC, et al. Effects of radiotherapy with concomitant and adjuvant temozolomide versus radiotherapy alone on survival in glioblastoma in a randomised phase III study: 5-year analysis of the EORTC-NCIC trial. Lancet Oncol 2009;10(5):459-66.
2. Hochberg FH, Pruitt A. Assumptions in the radiotherapy of glioblastoma. Neurology 1980;30(9):907-11.
3. Lee SW, Fraass BA, Marsh LH, Herbort K, Gebarski SS, Martel MK, et al. Patterns of failure following high-dose 3-D conformal radiotherapy for high-grade astrocytomas: a quantitative dosimetric study. Int J Radiat Oncol Biol Phys 1999;43(1):79-88.
4. Piccirillo SGM, Colman S, Potter NE, van Delft FW, Lillis S, Carnicer MJ, et al. Genetic and Functional Diversity of Propagating Cells in Glioblastoma. Stem cell report 2014;DOI:http://dx.doi.org/10.1016/j.stemcr.2014.11.003.
5. Sottoriva A, Spiteri I, Shibata D, Curtis C, Tavare S. Single-molecule genomic data delineate patient-specific tumor profiles and cancer stem cell organization. Cancer Res 2013;73(1):41-9.
6. Greaves M, Maley CC. Clonal evolution in cancer. Nature 2012;481(7381):306-13.
7. Galli R, Binda E, Orfanelli U, Cipelletti B, Gritti A, De Vitis S, et al. Isolation and characterization of tumorigenic, stem-like neural precursors from human glioblastoma. Cancer Res 2004;64(19):7011-21.
8. Singh SK, Hawkins C, Clarke ID, Squire JA, Bayani J, Hide T, et al. Identification of human brain tumour initiating cells. Nature 2004;432(7015):396-401.
9. Son MJ, Woolard K, Nam DH, Lee J, Fine HA. SSEA-1 is an enrichment marker for tumor-initiating cells in human glioblastoma. Cell Stem Cell 2009;4(5):440-52.
10. Bao S, Wu Q, McLendon RE, Hao Y, Shi Q, Hjelmeland AB, et al. Glioma stem cells promote radioresistance by preferential activation of the DNA damage response. Nature 2006;444(7120):756-60.
11. Cheng L, Huang Z, Zhou W, Wu Q, Donnola S, Liu JK, et al. Glioblastoma stem cells generate vascular pericytes to support vessel function and tumor growth. Cell 2013;153(1):139-52.
12. Velpula KK, Rehman AA, Chelluboina B, Dasari VR, Gondi CS, Rao JS, et al. Glioma stem cell invasion through regulation of the interconnected ERK, integrin alpha6 and N-cadherin signaling pathway. Cell Signal 2012;24(11):2076-84.
13. Liu G, Yuan X, Zeng Z, Tunici P, Ng H, Abdulkadir IR, et al. Analysis of gene expression and chemoresistance of CD133+ cancer stem cells in glioblastoma. Mol Cancer 2006;5:67.
14. Chen J, Li Y, Yu TS, McKay RM, Burns DK, Kernie SG, et al. A restricted cell population propagates glioblastoma growth after chemotherapy. Nature 2012;488(7412):522-6.
15. Smith J, Tho LM, Xu N, Gillespie DA. The ATM-Chk2 and ATR-Chk1 pathways in DNA damage signaling and cancer. Adv Cancer Res 2010;108:73-112.
16. Jazayeri A, Falck J, Lukas C, Bartek J, Smith GC, Lukas J, et al. ATM- and cell cycle-dependent regulation of ATR in response to DNA double-strand breaks. Nat Cell Biol 2006;8(1):37-45.
17. Myers JS, Cortez D. Rapid activation of ATR by ionizing radiation requires ATM and Mre11. J Biol Chem 2006;281(14):9346-50.
18. Byun TS, Pacek M, Yee MC, Walter JC, Cimprich KA. Functional uncoupling of MCM helicase and DNA polymerase activities activates the ATR-dependent checkpoint. Genes Dev 2005;19(9):1040-52.
19. MacDougall CA, Byun TS, Van C, Yee MC, Cimprich KA. The structural determinants of checkpoint activation. Genes Dev 2007;21(8):898-903.

20. Duursma AM, Driscoll R, Elias JE, Cimprich KA. A role for the MRN complex in ATR activation via TOPBP1 recruitment. Mol Cell 2013;50(1):116-22.
21. Boutros R, Lobjois V, Ducommun B. CDC25 phosphatases in cancer cells: key players? Good targets? Nat Rev Cancer 2007;7(7):495-507.
22. Carruthers R, Chalmers AJ. The potential of PARP inhibitors in neuro-oncology. CNS Oncol 2012;1(1):85-97.
23. Bartkova J, Hamerlik P, Stockhausen MT, Ehrmann J, Hlobilkova A, Laursen H, et al. Replication stress and oxidative damage contribute to aberrant constitutive activation of DNA damage signalling in human gliomas. Oncogene 2010;29(36):5095-102.
24. Galia A, Calogero AE, Condorelli R, Fraggetta F, La Corte A, Ridolfo F, et al. PARP-1 protein expression in glioblastoma multiforme. Eur J Histochem 2012;56(1):e9.
25. McCord AM, Jamal M, Williams ES, Camphausen K, Tofilon PJ. CD133+ glioblastoma stem-like cells are radiosensitive with a defective DNA damage response compared with established cell lines. Clin Cancer Res 2009;15(16):5145-53.
26. Ropolo M, Daga A, Griffero F, Foresta M, Casartelli G, Zunino A, et al. Comparative analysis of DNA repair in stem and nonstem glioma cell cultures. Mol Cancer Res 2009;7(3):383-92.
27. Carruthers R, Ahmed SU, Strathdee K, Gomez-Roman N, Amoah-Buahin E, Watts C, et al. Abrogation of radioresistance in glioblastoma stem-like cells by inhibition of ATM kinase. Mol Oncol 2014.
28. Curtin NJ. DNA repair dysregulation from cancer driver to therapeutic target. Nat Rev Cancer 2012;12(12):801-17.
29. Bartkova J, Horejsi Z, Koed K, Kramer A, Tort F, Zieger K, et al. DNA damage response as a candidate anti-cancer barrier in early human tumorigenesis. Nature 2005;434(7035):864-70.
30. Golding SE, Rosenberg E, Valerie N, Hussaini I, Frigerio M, Cockcroft XF, et al. Improved ATM kinase inhibitor KU-60019 radiosensitizes glioma cells, compromises insulin, AKT and ERK prosurvival signaling, and inhibits migration and invasion. Mol Cancer Ther 2009;8(10):2894-902.
31. Biddlestone-Thorpe L, Sajjad M, Rosenberg E, Beckta JM, Valerie NC, Tokarz M, et al. ATM kinase inhibition preferentially sensitizes p53-mutant glioma to ionizing radiation. Clin Cancer Res 2013;19(12):3189-200.
32. Eich M, Roos WP, Nikolova T, Kaina B. Contribution of ATM and ATR to the resistance of glioblastoma and malignant melanoma cells to the methylating anticancer drug temozolomide. Mol Cancer Ther 2013;12(11):2529-40.
33. Dungey FA, Loser DA, Chalmers AJ. Replication-dependent radiosensitization of human glioma cells by inhibition of poly(ADP-Ribose) polymerase: mechanisms and therapeutic potential. Int J Radiat Oncol Biol Phys 2008;72(4):1188-97.
34. Hirose Y, Berger MS, Pieper RO. Abrogation of the Chk1-mediated G(2) checkpoint pathway potentiates temozolomide-induced toxicity in a p53-independent manner in human glioblastoma cells. Cancer Res 2001;61(15):5843-9.
35. Venere M, Hamerlik P, Wu Q, Rasmussen RD, Song LA, Vasanji A, et al. Therapeutic targeting of constitutive PARP activation compromises stem cell phenotype and survival of glioblastoma-initiating cells. Cell Death Differ 2014;21(2):258-69.
36. Fael Al-Mayhani TM, Ball SL, Zhao JW, Fawcett J, Ichimura K, Collins PV, et al. An efficient method for derivation and propagation of glioblastoma cell lines that conserves the molecular profile of their original tumours. J Neurosci Methods 2009;176(2):192-9.
37. Mannino M, Gomez-Roman N, Hochegger H, Chalmers AJ. Differential sensitivity of Glioma stem cells to Aurora kinase A inhibitors: implications for stem cell mitosis and centrosome dynamics. Stem Cell Res 2014;13(1):135-43.
38. Comprehensive genomic characterization defines human glioblastoma genes and core pathways. Nature 2008;455(7216):1061-8.

39. Guzi TJ, Paruch K, Dwyer MP, Labroli M, Shanahan F, Davis N, et al. Targeting the replication checkpoint using SCH 900776, a potent and functionally selective CHK1 inhibitor identified via high content screening. Mol Cancer Ther 2011;10(4):591-602.
40. Montano R, Chung I, Garner KM, Parry D, Eastman A. Preclinical development of the novel Chk1 inhibitor SCH900776 in combination with DNA-damaging agents and antimetabolites. Mol Cancer Ther 2012;11(2):427-38.
41. Leung-Pineda V, Ryan CE, Piwnica-Worms H. Phosphorylation of Chk1 by ATR is antagonized by a Chk1-regulated protein phosphatase 2A circuit. Mol Cell Biol 2006;26(20):7529-38.
42. Bartek J, Lukas J. Chk1 and Chk2 kinases in checkpoint control and cancer. Cancer Cell 2003;3(5):421-9.
43. Liu Q, Guntuku S, Cui XS, Matsuoka S, Cortez D, Tamai K, et al. Chk1 is an essential kinase that is regulated by Atr and required for the G(2)/M DNA damage checkpoint. Genes Dev 2000;14(12):1448-59.
44. Tse AN, Rendahl KG, Sheikh T, Cheema H, Aardalen K, Embry M, et al. CHIR-124, a novel potent inhibitor of Chk1, potentiates the cytotoxicity of topoisomerase I poisons in vitro and in vivo. Clin Cancer Res 2007;13(2 Pt 1):591-602.
45. Wang J, Sakariassen PO, Tsinkalovsky O, Immervoll H, Boe SO, Svendsen A, et al. CD133 negative glioma cells form tumors in nude rats and give rise to CD133 positive cells. Int J Cancer 2008;122(4):761-8.
46. Suva ML, Rheinbay E, Gillespie SM, Patel AP, Wakimoto H, Rabkin SD, et al. Reconstructing and reprogramming the tumor-propagating potential of glioblastoma stem-like cells. Cell 2014;157(3):580-94.
47. Vlashi E, Kim K, Lagadec C, Donna LD, McDonald JT, Eghbali M, et al. In vivo imaging, tracking, and targeting of cancer stem cells. J Natl Cancer Inst 2009;101(5):350-9.
48. Cruceru ML, Neagu M, Demoulin JB, Constantinescu SN. Therapy targets in glioblastoma and cancer stem cells: lessons from haematopoietic neoplasms. J Cell Mol Med 2013;17(10):1218-35.
49. Ghosal G, Chen J. DNA damage tolerance: a double-edged sword guarding the genome. Transl Cancer Res 2013;2(3):107-29.
50. Fokas E, Prevo R, Pollard JR, Reaper PM, Charlton PA, Cornelissen B, et al. Targeting ATR in vivo using the novel inhibitor VE-822 results in selective sensitization of pancreatic tumors to radiation. Cell Death Dis 2012;3:e441.

Figure legends

Figure 1. GSCs are radioresistant with defective DDR

(A) Enrichment of stem cell markers SOX2, Nestin, CD133 and Olig2 under GSC culture conditions compared to paired bulk populations of primary patient derived GBM cell lines. **(B)** Flow cytometry plots and summary showing relative expression of CD133 and CD15 in E2 and G7 GSC and bulk populations. **(C-D)** Clonogenic survival assays showing E2 and G7 GSCs are more radioresistant than paired bulk populations. **(E)** Calculation of dose modifying factor (DMF) at 37% survival comparing E2 and G7 GSC vs bulk populations and *p* values associated with comparisons of DMF. **(F)** Plots summarising combined annexin V and PI staining or **(G)** fold induction in caspase 3/7 activity at 48 hours in E2 and G7 GSC and bulk populations following treatment with 15 or 30 Gy ionising radiation. Error bars show mean ± SEM from n=3 independent experiments, * $p<0.05$, NS=non-significant.

Figure 2. GSCs have upregulated DDR proteins under basal condition and active CHK1 rapidly following IR

(A) Analysis of multiple DDR proteins under basal conditions in GSC or bulk populations in a panel of primary patient derived GBM cell lines. Loading control as shown in Figure 1A. **(B)** Analysis of total and phosphorylated CHK1 in CD133 or CD15 sorted cell populations. Flow cytometry plots show post-sort analysis of G7 cells sorted by CD15 expression. **(C)** Cell cycle distribution and profiles of E2 GSC and bulk populations. **(D)** Immunohistochemistry analysis of orthotopic tumour sections generated from E2 and G7 orthotopic xenografts and a GBM patient specimen showing PARP1 and p-ATM staining. **(E)** Western blots showing rapid activation of DNA damage response markers at early time points in E2 GSC compared to bulk populations following 5Gy IR. **(F)** Fold induction in CHK1 activation relative to untreated cells following quantification of p-CHK1(S345):CHK1 ratios from immunoblots after radiation. Error bars show mean + SEM from three independent experiments. **(G)** 24 hour time course highlighting CHK1 and phosporylated CHK1 levels in E2 and G7 paired GSC and bulk populations following 5Gy IR. **(H)** Response of E2 bulk and GSC populations to various activators of CHK1: IR=5Gy, 1hr; UV=$10JM^{-2}$, 1hr; HU=10mM, 3hr; Aphidicolin=1mM, 3hr, (* longer exposure).

Figure 3. Rapid activation of G2/M cell cycle checkpoint in GSCs following IR

Summary of flow cytometry data analysing mitotic p-His H3 S10 cell population to measure G2/M cell cycle checkpoint in paired E2 and G7 GSC and bulk populations. **(A)** 3 hour time course following 5Gy IR treatment showing a rapid activation of G2/M checkpoint in GSCs as measured by the time required to reduce mitotic population by 50%. **(B)** IR dose response showing E2 and G7 GSC populations require significantly lower dose of radiation compared to the bulk cells to activate G2/M checkpoint by 75% relative to unirradiated cells. **(C)** 12 hour IR time course showing E2 and G7 bulk cells exit the G2/M checkpoint significantly quicker than the paired GSC population as measured by the time required for mitotic cell population to return to baseline levels. Plots show mean ± SEM, $n\geq3$ independent experiments.

Figure 4. GSCs are radiosensitised by the CHK1 inhibitor SCH900776 (SCH)

(A) Inhibition of CHK1 in E2 GSCs following 1 hr pre-treatment with various concentrations of SCH followed by 120Jcm^{-2} UV for 1hr. **(B)** Time course showing abrogation of IR induced CHK1 activation by pre-treatment of E2 GSCs with 3μM of SCH for 1hr (* denotes longer exposure). **(C)** Analysis of multiple biomarkers of CHK1 inhibition at 24 hours in E2 GSCs treated with various concentrations of SCH for 1hr followed by 5Gy IR. **(D)** Plots summarising flow cytometry data showing inhibition of IR induced G2/M checkpoint activation in E2 and G7 GSCs treated with 3μM SCH for 1hr followed by 5Gy IR, (mean ± SEM from n≥3 independent experiments, *p<0.05, **p<0.01,***p<0.001 relative to IR alone. **(E)** Clonogenic survival curves showing radiosensitisation of E2 and G7 GSC and bulk populations following 3μM of SCH treatment. **(F)** Summary of clonogenic data showing SER of GSC and bulk populations at 37% survival and SF at 4Gy in the presence or absence of SCH. * denotes p<0.05 based on the 95% confidence intervals between SER of GSCs and bulk population or SF of GSC or bulk populations plus or minus SCH treatment. NS=Non significant.

Figure 5. Inhibition of CHK1 increases DNA damage, induces mitotic catastrophe and leads to genomic instability in irradiated GSC

(A) Representative flow cytometry plots showing the total percentage of γ-H2AX positive cells in E2 GSC 24 hours after 3μM SCH treatment for 1 hr followed by 5Gy IR. **(B)** Bar chart summarising the percentage of total γ-H2AX positive cells at 24 hours following treatment of E2 GSCs with various concentrations of SCH +/- 5 Gy, error bars show mean + SEM, n≥3 independent experiments, *p<0.05. **(C)** Representative histogram plots from flow cytometry data showing the percentage of mitotic cells with high γ-H2AX at 24 hours following treatment with 3μM SCH and 5Gy IR. **(D)** Summary of flow cytometry data showing percentage of mitotic cells with high γ-H2AX at 24 hours following treatment of E2 GSC with various concentrations of SCH, error bars show mean + SEM, n≥3 independent experiments, *p<0.05, **p<0.01. **(E)** Representative immunofluorescence images showing p-His H3 positive mitotic cells (green) with no/low γ-H2AX (red, top panel) or high γ-H2AX (middle panel). Image of cell undergoing mitotic catastrophe as marked by nuclear blebbing and high γ-H2AX (bottom panel). DAPI nuclear stain in blue. Bar charts summarising immunofluorescence data from analysis of ~75 mitotic cells. **(F)** Representative image and summary of the percentage of E2 GSCs with micronuclei (arrows) 24 hours following treatment with 3μM SCH +/- 5 Gy, error bars show mean + SEM from scoring ~ 500 nuclei, *p<0.05, **p<0.01).

Figure 6. GSC show enhanced DNA repair capacity following irradiation and/or CHK1 inhibition

Summary of flow cytometry data showing the percentage of **(A)** γ-H2AX positive cells, **(B)** mitotic cells with high γ-H2AX and **(C)** mitotic catastrophe (arrows) in paired G7 bulk and GSC populations at 24 hours following treatment with 3μM SCH and/or 5Gy IR, error bars show mean + SEM, n≥3 independent experiments, **p<0.01, **p<0.001. **(D)** Bar chart summary of the percentage of G7 bulk and GSC with micronuclei 24 hours following the indicated treatment combinations, error bars show mean + SEM from scoring ~ 600 nuclei, ***p<0.001. **(E)** Representative immunofluorescence images of E2 GSC and bulk populations at 24 hours following 10Gy IR, γ-H2AX foci (green), CENPF (red) and DAPI

(blue). **(F)** Plots showing median γ-H2AX foci per nucleus in E2 bulk and GSC CENPF positive or negative cells populations from scoring a minimum 65 (CENPF positive) or 300 (CENPF negative) nuclei, *p<0.05, **p<0.01.

Figure 7. Enhanced radiosensitisation of GSCs by parallel inhibition of DNA repair and cell cycle checkpoint pathways

(A-B) Clonogenic survival curves in E2 GSC and bulk populations following treatment with multiple DDRi in combination with radiation. **(B)** Summary of SER at 37% survival in paired populations with 95% confidence intervals, *p<0.05 and NS=non-significant between GSC and bulk population. CHK1i data as shown previously in Figure 4E & 4F. **(C)** Inhibition of radiation induced G2/M checkpoint activation in E2 GSCs following 5Gy IR treatment in the presence of various DDRi, significance relative to DMSO treatment (IR alone); *p<0.05, **p<0.01, ***p<0.001. **(D)** Plots showing median number of γ-H2AX foci in CENPF positive cells at 24 hours following treatment with IR in combination with DDRi, minimum of 65 nuclei scored; ***p<0.001. **(E)** Clonogenic survival curves in E2 cells showing significant radiosensitisation of GSC over the bulk population as shown by the SER following combined treatment with ATR+PARP inhibitors in combination with radiation. ATMi data as shown in part A and B. **(F)** Neurosphere formation assay showing maximum reduction in the number of neurospheres at 4 weeks following ATR+PARP1 inhibition in combination with radiation; **p<0.01, ***p<0.001.

Figure 1

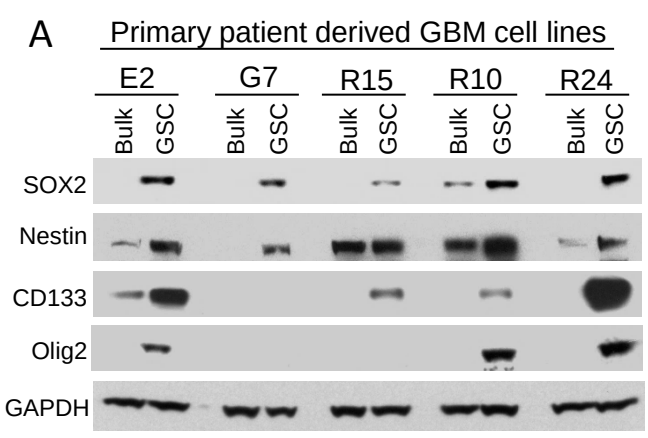

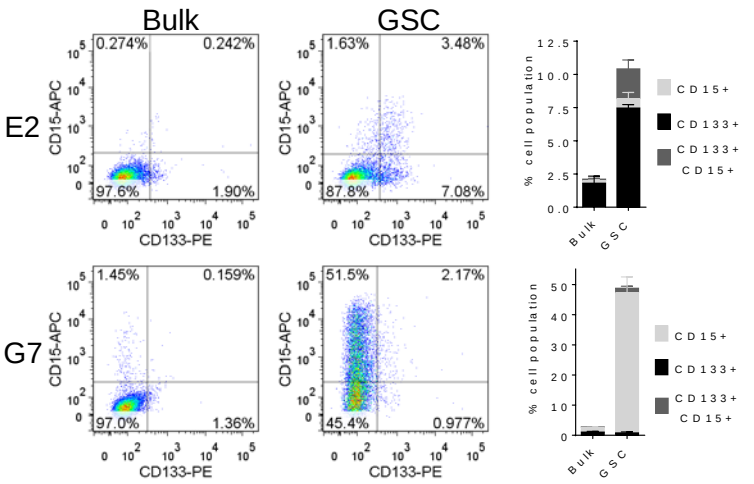

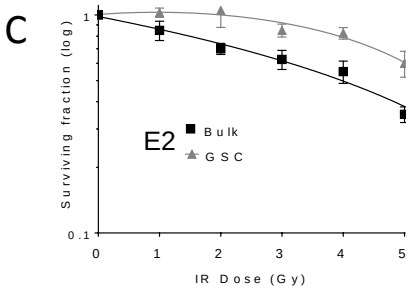

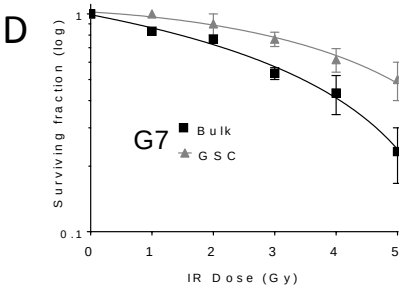

E

	DMF 0.37 (95% CI) *P* value
E2 GSC vs Bulk	1.36 (1.15, 1.57) p = 0.001
G7 GSC vs Bulk	1.44 (1.22, 1.66) p < 0.001

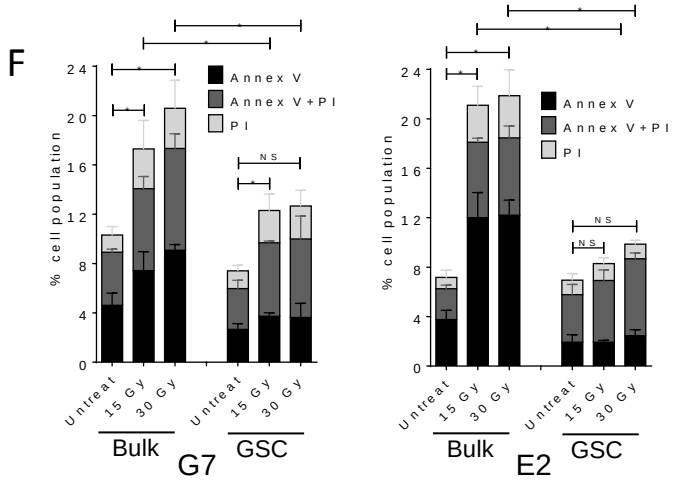

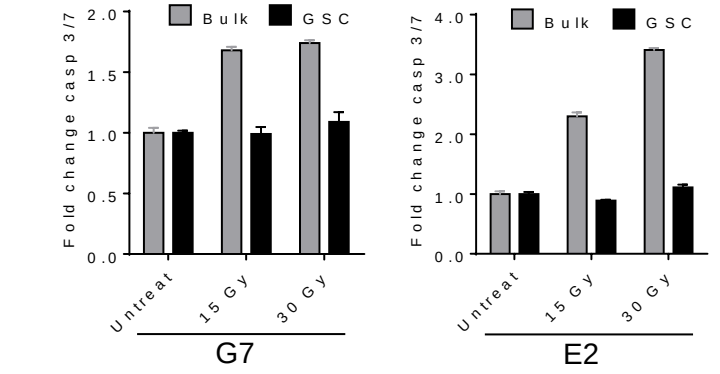

Figure 2

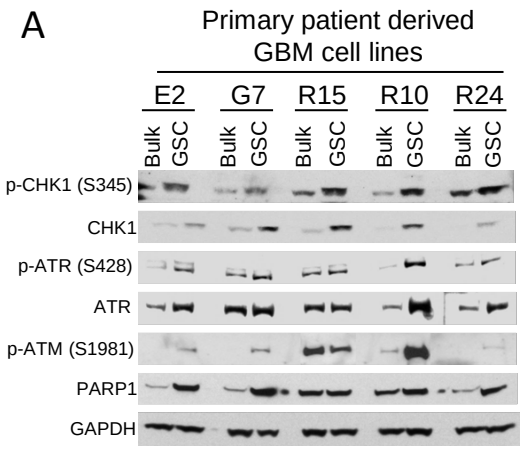

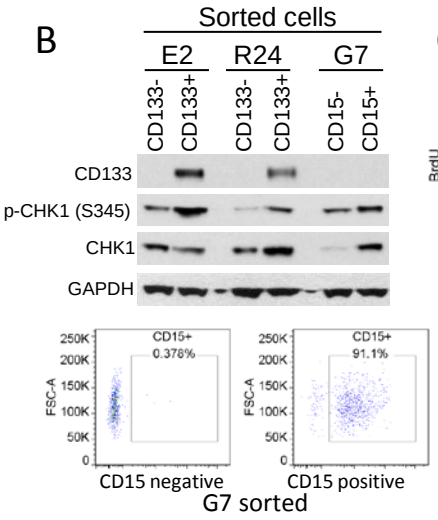

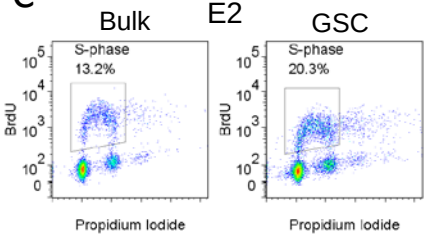

	Bulk	GCS
G1	74±5	58±6
S	13±3	20±5
G2/M	11±4	17±2

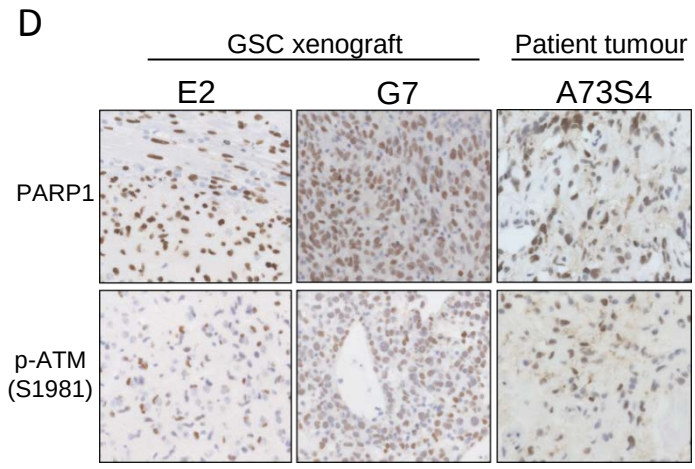

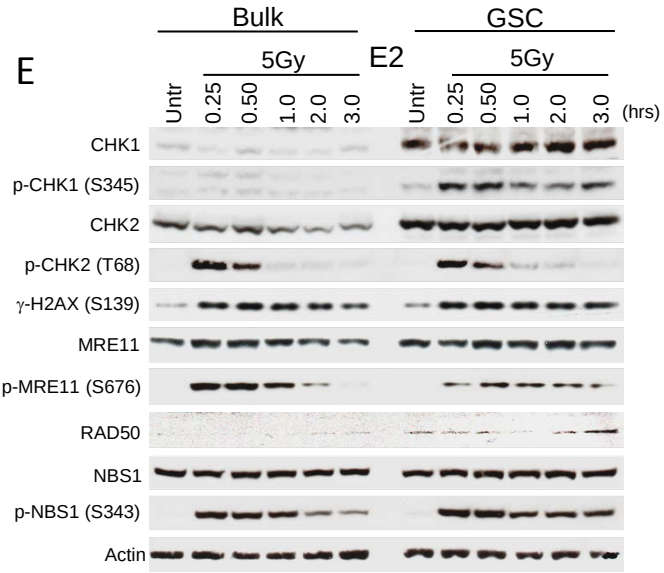

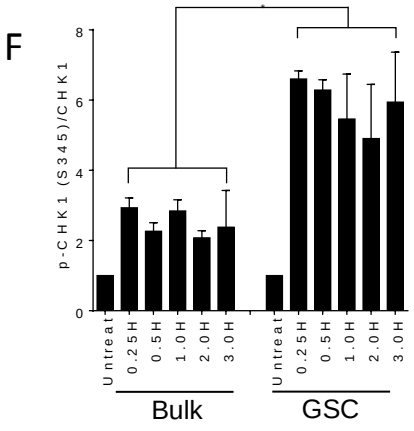

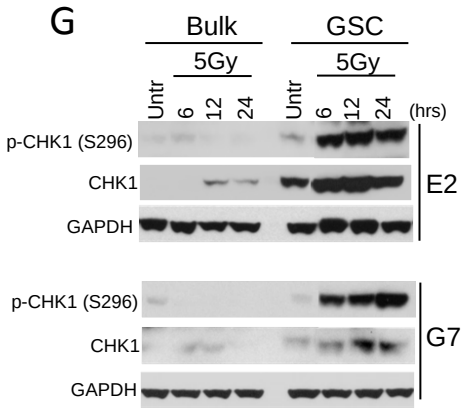

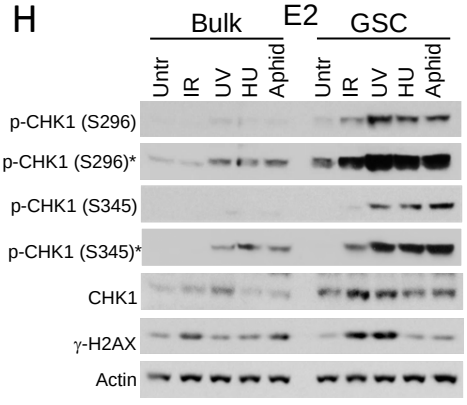

Figure 3

A

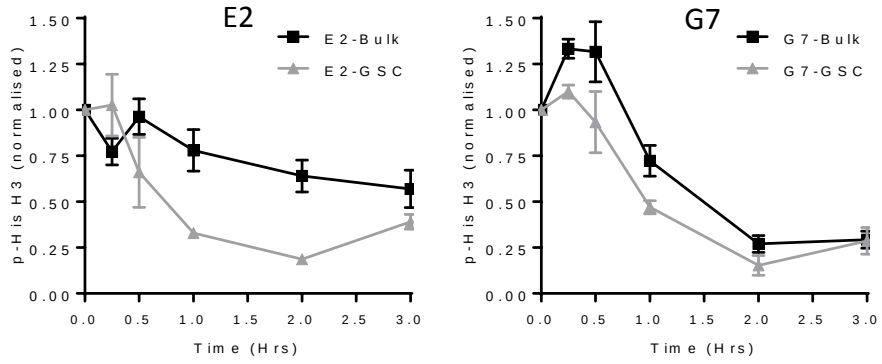

$G2/M_{50}$ Index (t=min)
50% reduction in mitotic cells

	Bulk	GSC	*p*
E2	>180	39±11	NA
G7	87±13	58±6	0.027

B

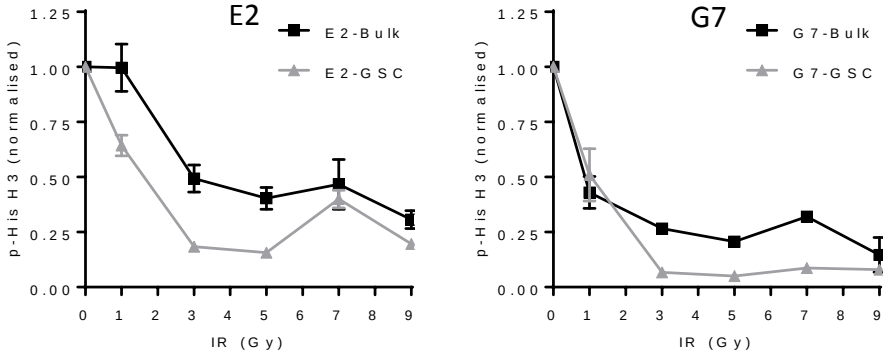

$G2/M_{75}$ Index (Gy)
75% reduction in mitotic cells

	Bulk	GSC	*p*
E2	5.3±1.8	2.6±0.1	0.042
G7	3.4±0.3	1.5±0.6	0.019

C

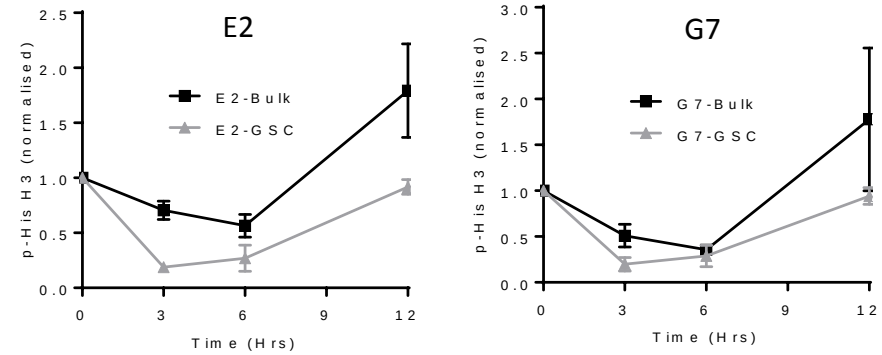

G2/M release (t=min)
Return to baseline mitotic levels

	Bulk	GSC	*p*
E2	513±48	859±28	0.030
G7	557±75	802±25	0.040

Figure 4

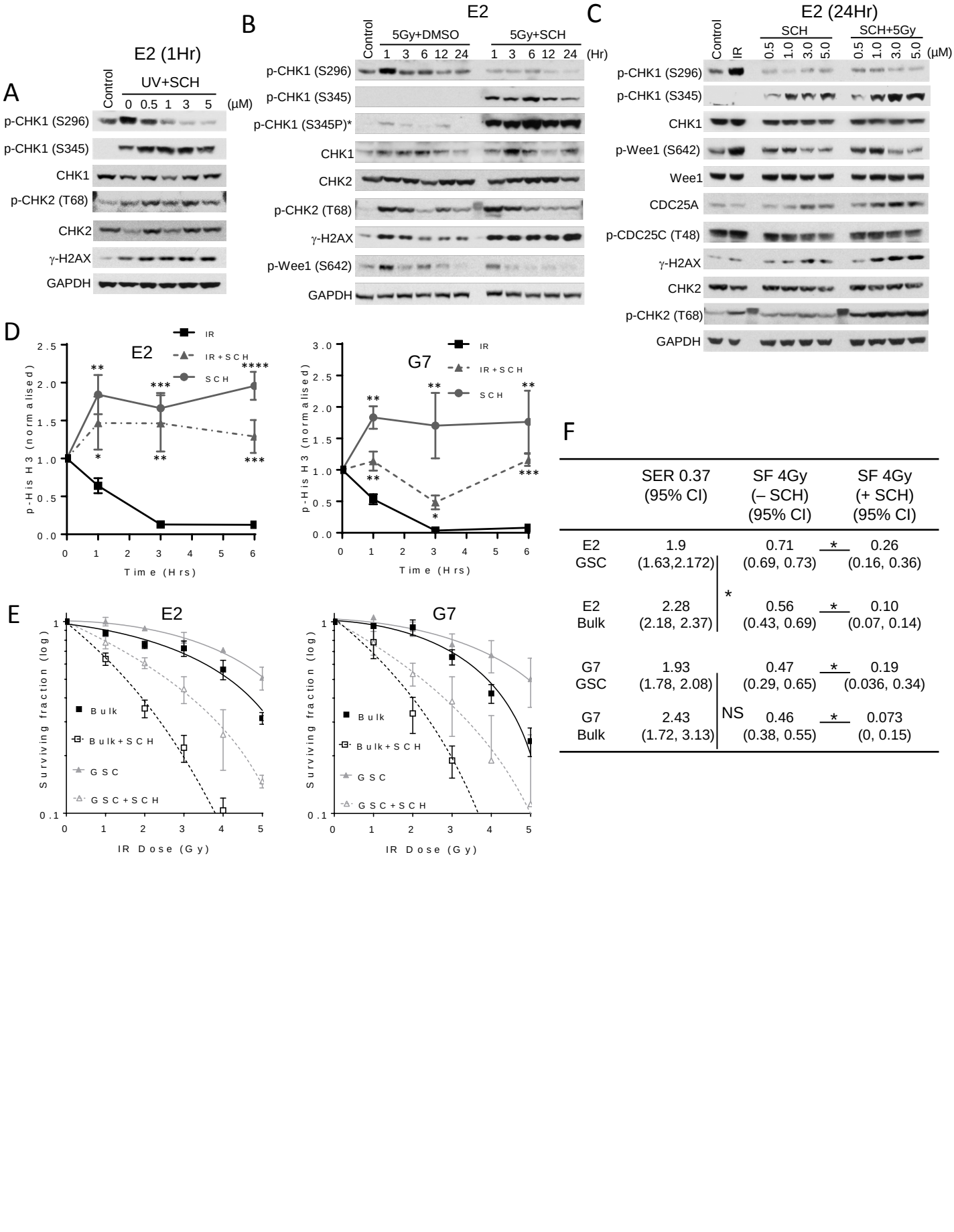

F

	SER 0.37 (95% CI)		SF 4Gy (– SCH) (95% CI)		SF 4Gy (+ SCH) (95% CI)
E2 GSC	1.9 (1.63,2.172)	*	0.71 (0.69, 0.73)	*	0.26 (0.16, 0.36)
E2 Bulk	2.28 (2.18, 2.37)	*	0.56 (0.43, 0.69)	*	0.10 (0.07, 0.14)
G7 GSC	1.93 (1.78, 2.08)		0.47 (0.29, 0.65)	*	0.19 (0.036, 0.34)
G7 Bulk	2.43 (1.72, 3.13)	NS	0.46 (0.38, 0.55)	*	0.073 (0, 0.15)

Figure 5

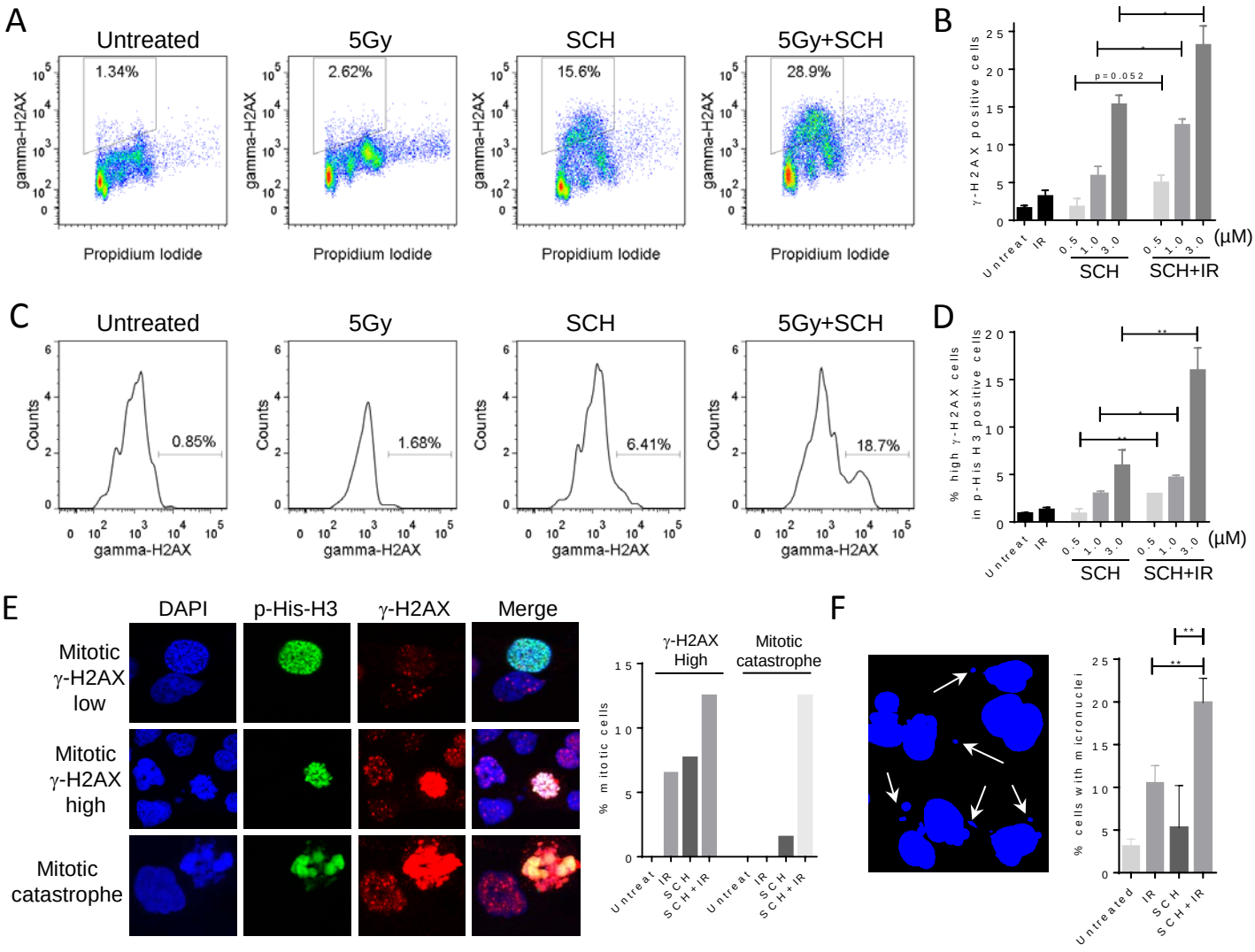
A
Untreated
5Gy
SCH
5Gy+SCH
1.34%
2.62%
15.6%
28.9%
gamma-H2AX
Propidium Iodide
B
γ-H2AX positive cells
p=0.052
Untreat
IR
0.5
1.0
3.0
SCH
SCH+IR
(μM)
C
Untreated
5Gy
SCH
5Gy+SCH
Counts
0.85%
1.68%
6.41%
18.7%
gamma-H2AX
D
% high γ-H2AX cells in p-His H3 positive cells
E
DAPI
p-His-H3
γ-H2AX
Merge
Mitotic γ-H2AX low
Mitotic γ-H2AX high
Mitotic catastrophe
γ-H2AX High
Mitotic catastrophe
% mitotic cells
Untreat
IR
SCH
SCH+IR
F
% cells with micronuclei
Untreated

Figure 6

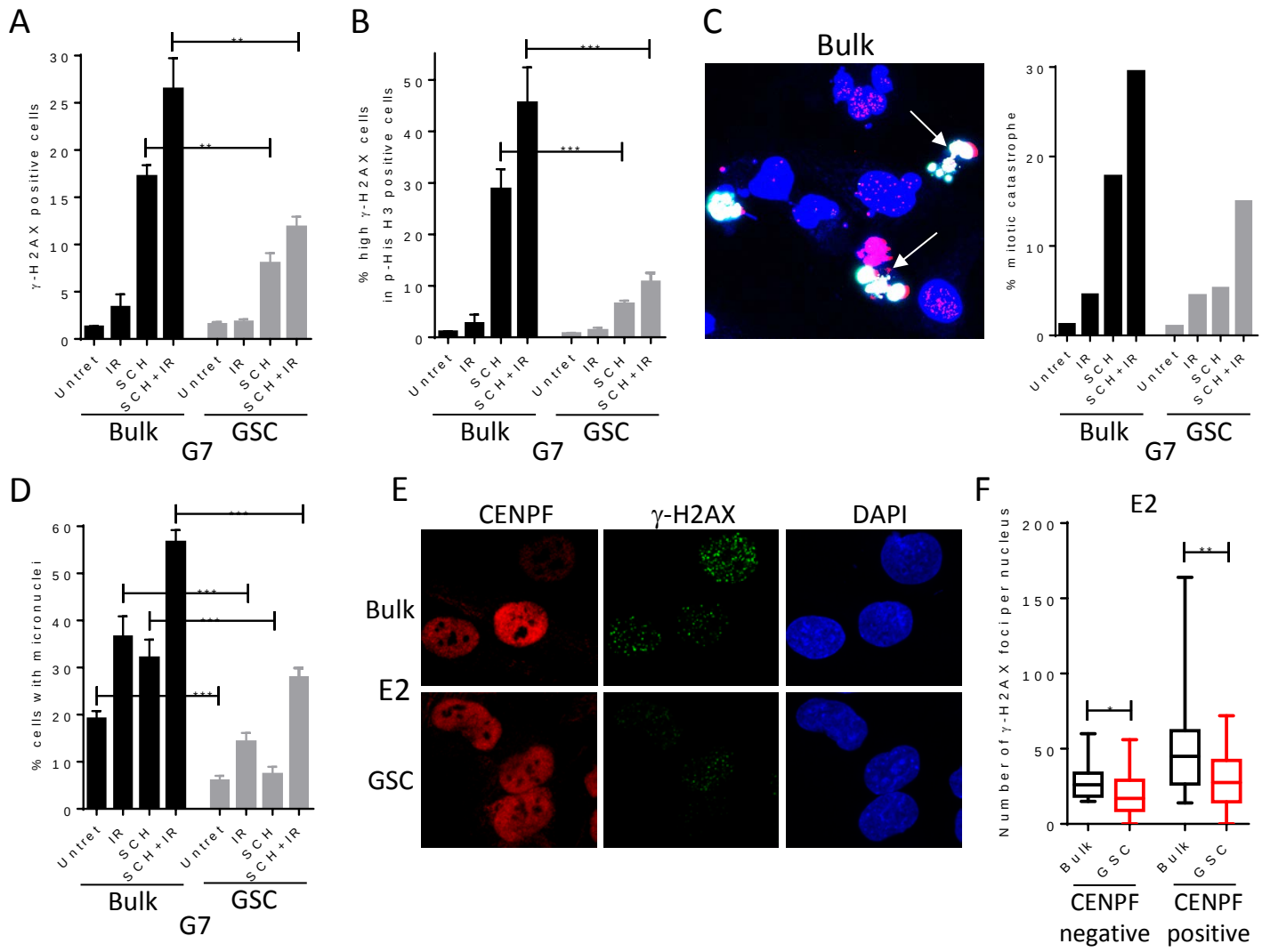
A
γ-H2AX positive cells
Untret
IR
SCH
SCH+IR
Bulk
GSC
G7
B
% high γ-H2AX cells in p-His H3 positive cells
C
Bulk
% mitotic catastrophe
D
% cells with micronuclei
E
CENPF
γ-H2AX
DAPI
Bulk
E2
GSC
F
E2
Number of γ-H2AX foci per nucleus
CENPF negative
CENPF positive

Figure 7

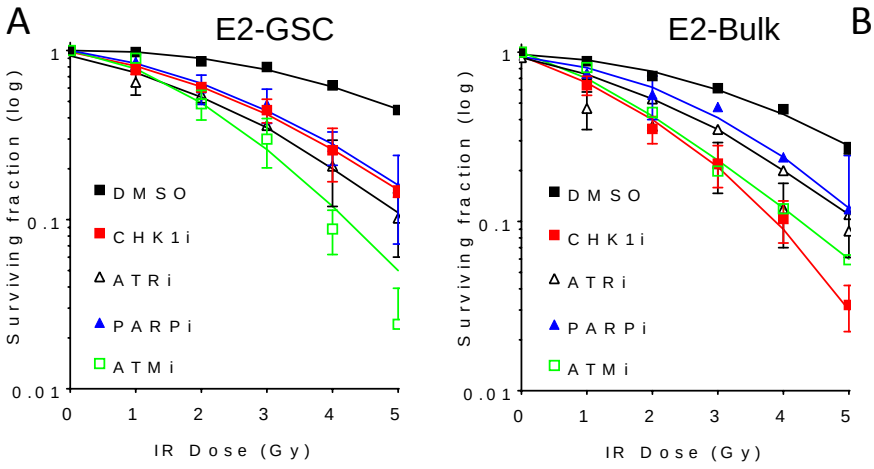

B

	GSC SER 0.37 (95% CI)	Bulk SER 0.37 (95% CI)	GSC vs Bulk
CHK1i	1.90 (1.63,2.17)	2.28 (2.18,2.37)	*
ATRi	2.00 (1.86, 2.10)	2.56 (1.78,3.34)	NS
PARPi	1.93 (1.23, 2.64)	1.34 (1.19, 1.48)	NS
ATMi	2.60 (1.72,3.40)	2.01 (1.27,2.86)	NS

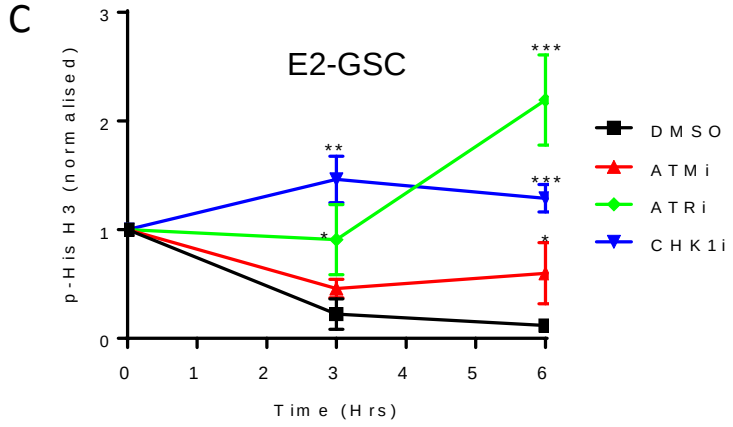

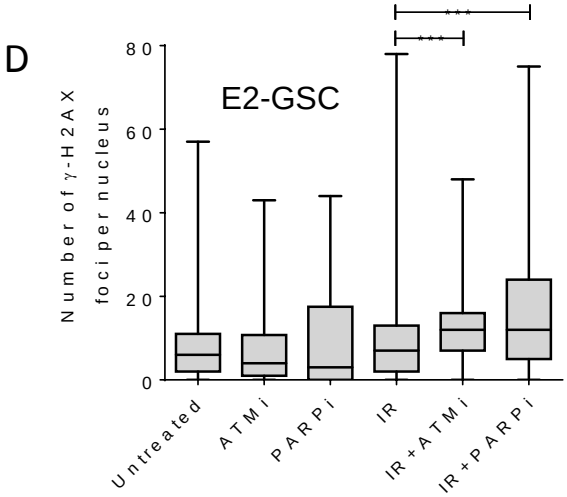

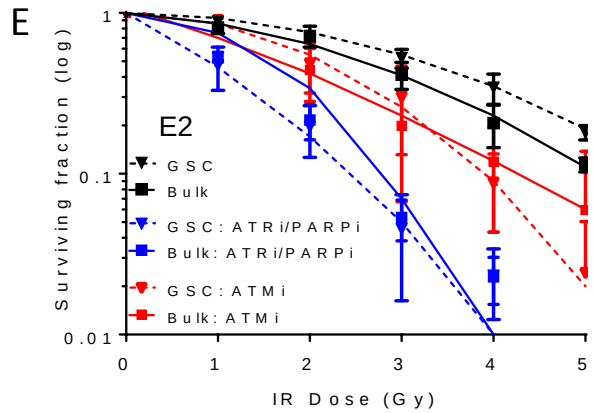

	GSC SER 0.37 (95% CI)	Bulk SER 0.37 (95% CI)	GSC vs Bulk
ATMi	2.60 (1.72,3.40)	2.01 (1.27,2.86)	NS
ATRi+ PARPi	3.20 (2.53, 3.95)	1.65 (1.46,1.89)	*

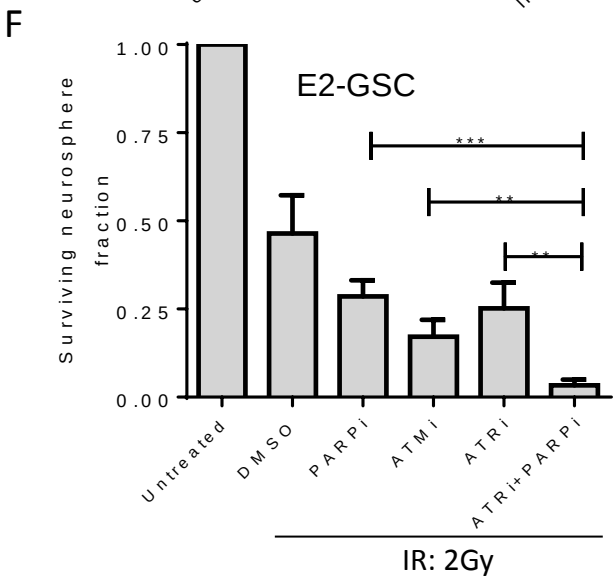

Supplementary Table 1

	E2 GSC	E2 bulk	G7 GSC	G7 bulk
Mean SF4Gy (95% CI)	0.78 (0.72, 0.83)	0.56 (0.47, 0.64)	0.65 (0.57,0.72)	0.43 (0.34,0.51)
T test of means	p = 0.001		p = 0.002	

Supplementary Table 1.
Analysis of clonogenics survival curves from Figure 1C and 1D showing colony surviving fractions at 4Gy in E2 and G7 bulk and GSC populations with 95% confidence interval and p-values based on t-test of means.

Supplementary Figure S1

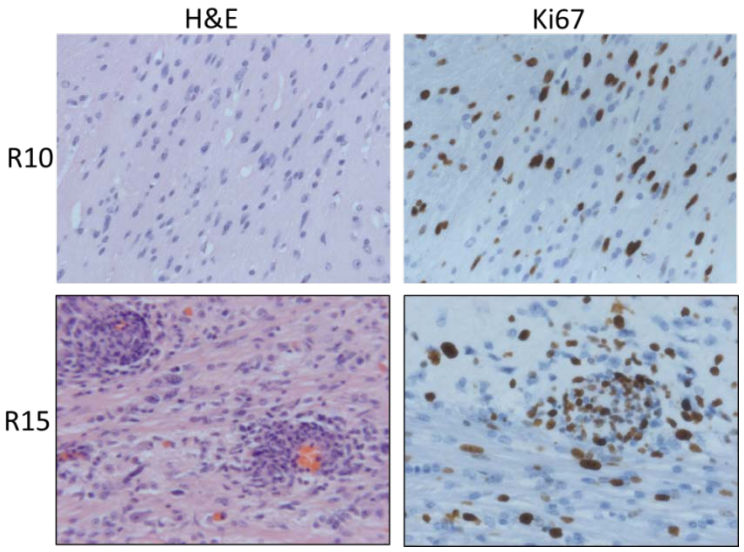

Supplementary Figure S1. Generation of orthotopic tumours from R10 and R15 GSCs
Immunohistochemistry images of tumour sections stained with Hematoxylin and eosin (H&E) showing tumour cell morphology and Ki67 showing proliferating tumour cells

Supplementary Figure S2

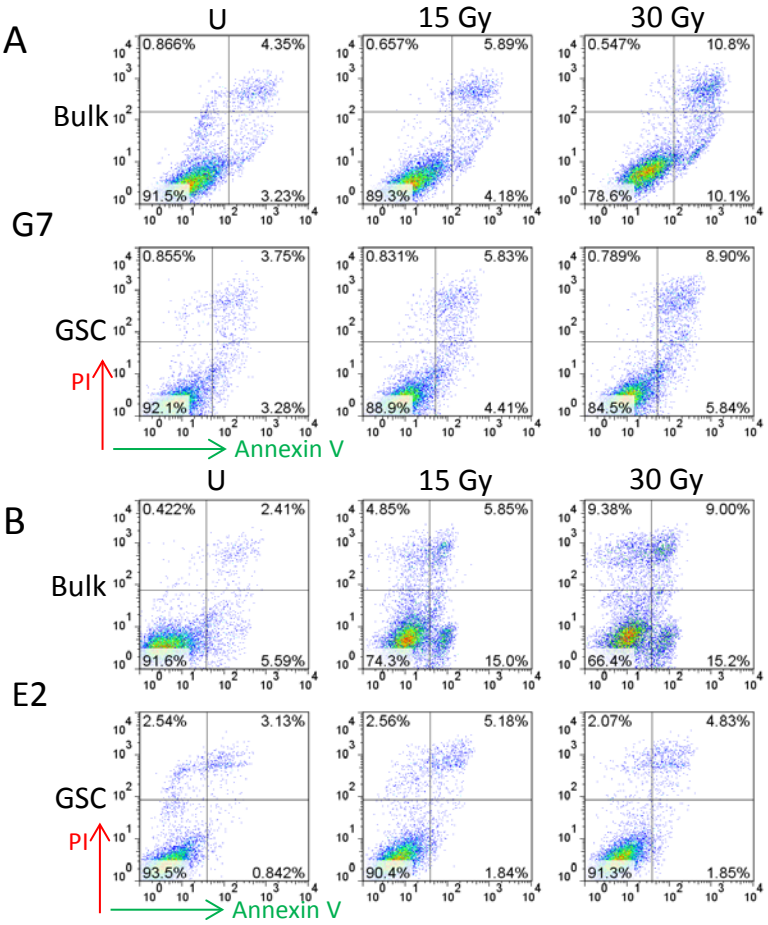

Supplementary Figure S2. GSCs are more resistant to IR induced cell death than bulk populations

(A-B) Flow cytometry plots showing percentage of annexin V and PI staining in G7 and E2 GSC and bulk populations following 48 hours treatment with 15 or 30 Gy IR.

Supplementary Figure S3

A

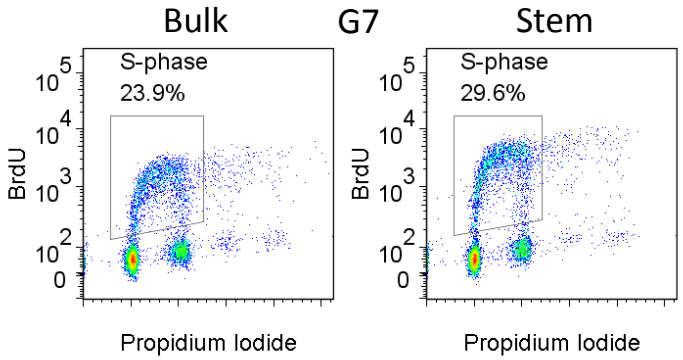

G7	Bulk	GCS
G1	60±6	54±6
S	18±3	23±4
G2/M	17±3	20±4

B

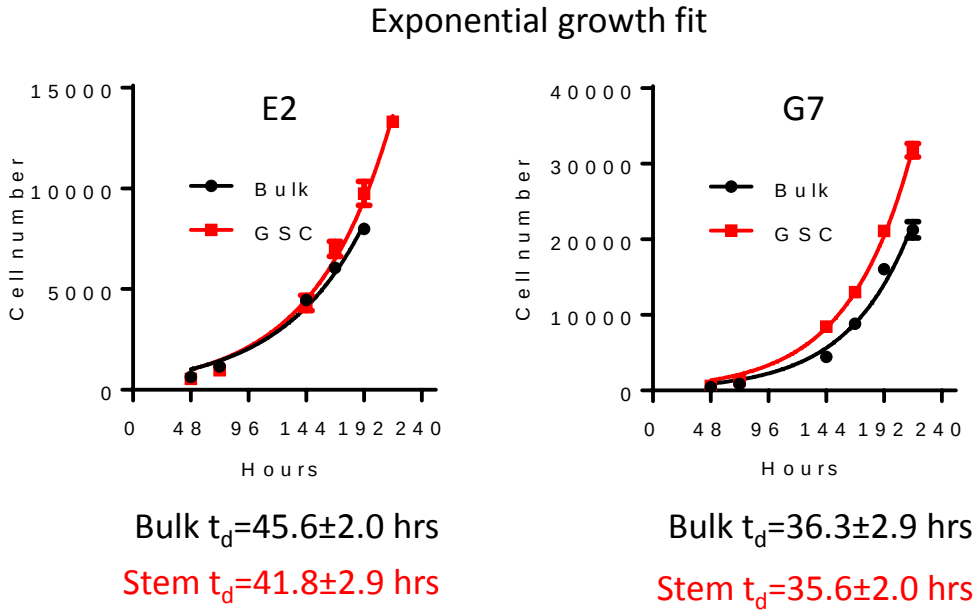

Bulk t_d=45.6±2.0 hrs

Stem t_d=41.8±2.9 hrs

Bulk t_d=36.3±2.9 hrs

Stem t_d=35.6±2.0 hrs

Supplementary Figure S3. Cell cycle profile and proliferation rates of GSC and bulk population **(A)** Representative BrdU cell cycle profiles and summary of cell cycle distribution in untreated G7 GSC and bulk population. **(B)** Cell growth curves with exponential growth fit measuring cell doubling rates in GSC and the bulk populations in E2 and G7 cell lines.

Supplementary Figure S4

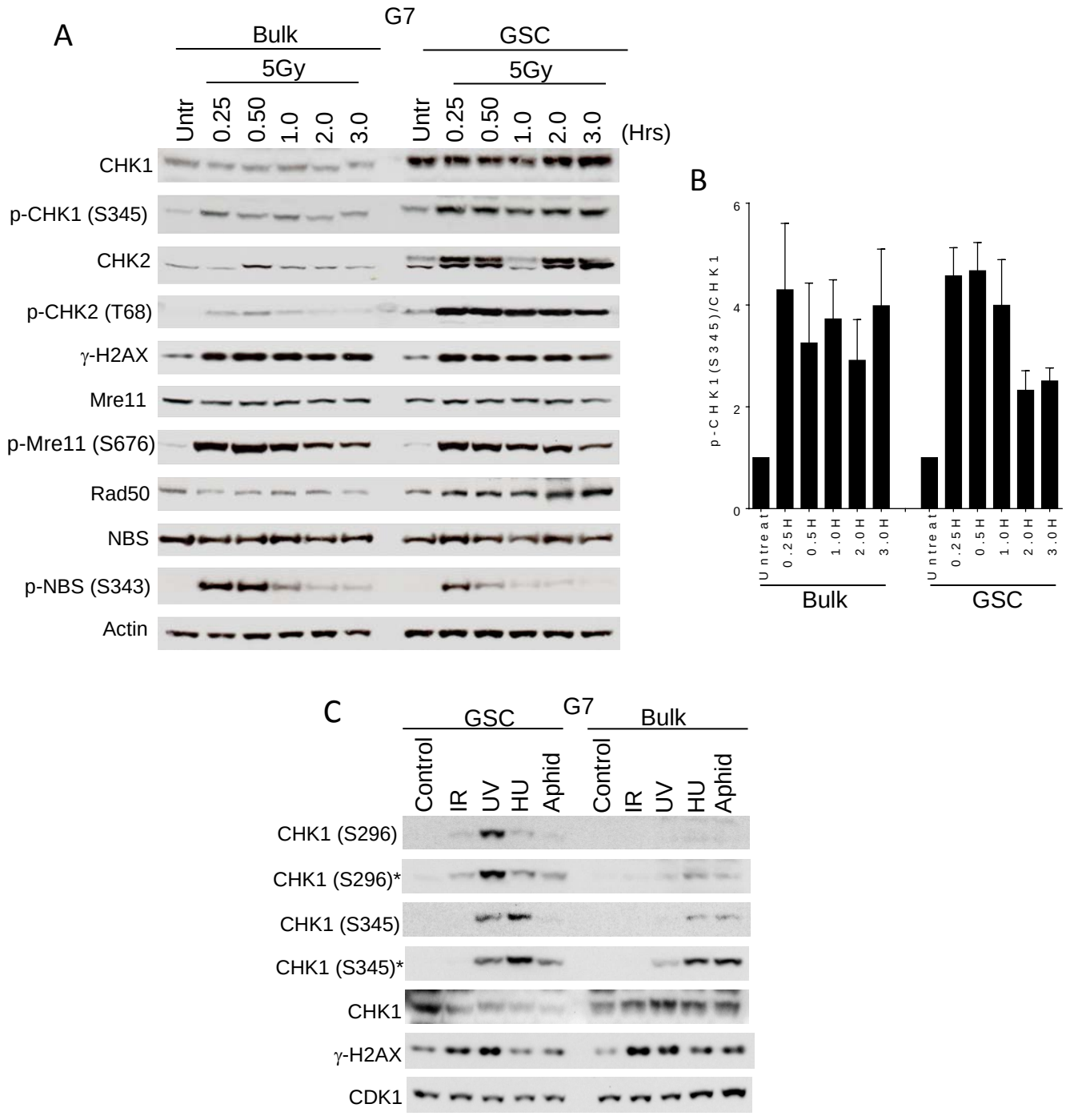

Supplementary Figure S4. Enhanced activation of CHK1 in GSCs
(A) Western blots showing activation of DNA damage response markers at early time points in G7 bulk and GSC population following 5Gy IR. **(B)** Fold induction in CHK1 activation at various time points following quantification of p-CHK1(S345)/CHK1 immunoblots in irradiated G7 bulk and GSCs. Untreated conditions normalised to 1, error bars show mean + SD from three independent experiments, **(C)** Response of G7 bulk and paired GSC populations to various activators of CHK1: IR=5Gy, 1hr; UV=10JM^{-2}, 1hr; HU=10mM, 3hr; Aphidicolin=1mM, 3hr, (* longer exposure).

Supplementary Figure S5

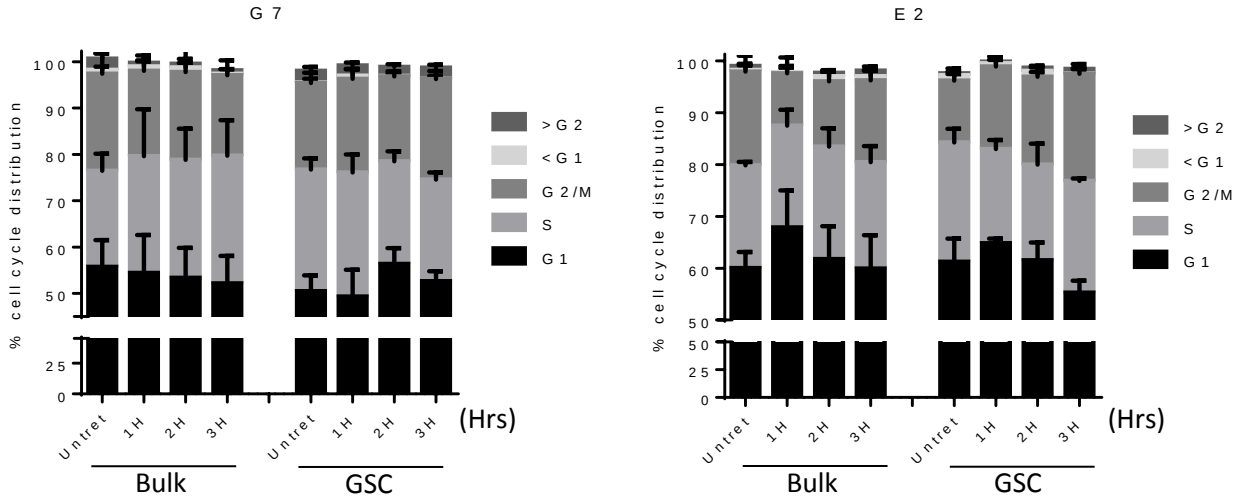

Supplementary Figure S5. Absence of G1 cell cycle checkpoint in irradiated GBM cell lines
Cell cycle distribution in G7 and E2 paired GSC and bulk population following 5Gy IR treatment at the time points indicated.

Supplementary Figure S6

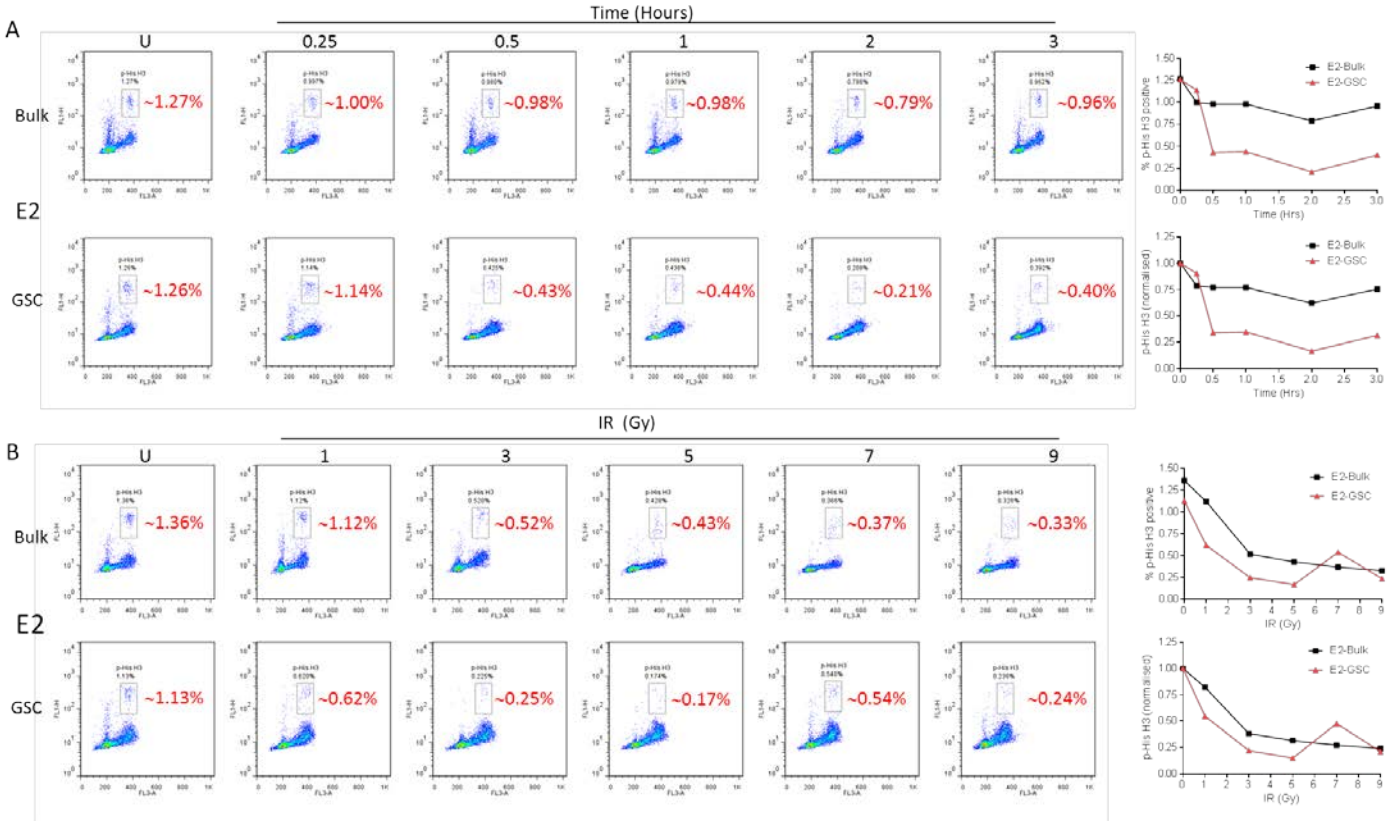

Supplementary Figure S6. Analysis of G2/M cell cycle checkpoint
Representative flow cytometry plots showing the percentage of mitotic p-His H3 S10 cells in E2 GSCs and bulk population following **(A)** 5Gy IR (time course) and **(B)** IR dose response (3 hours). Graphs show the actual (top) and normalised (bottom) p-His H3 S10 levels.

Supplementary Figure S7

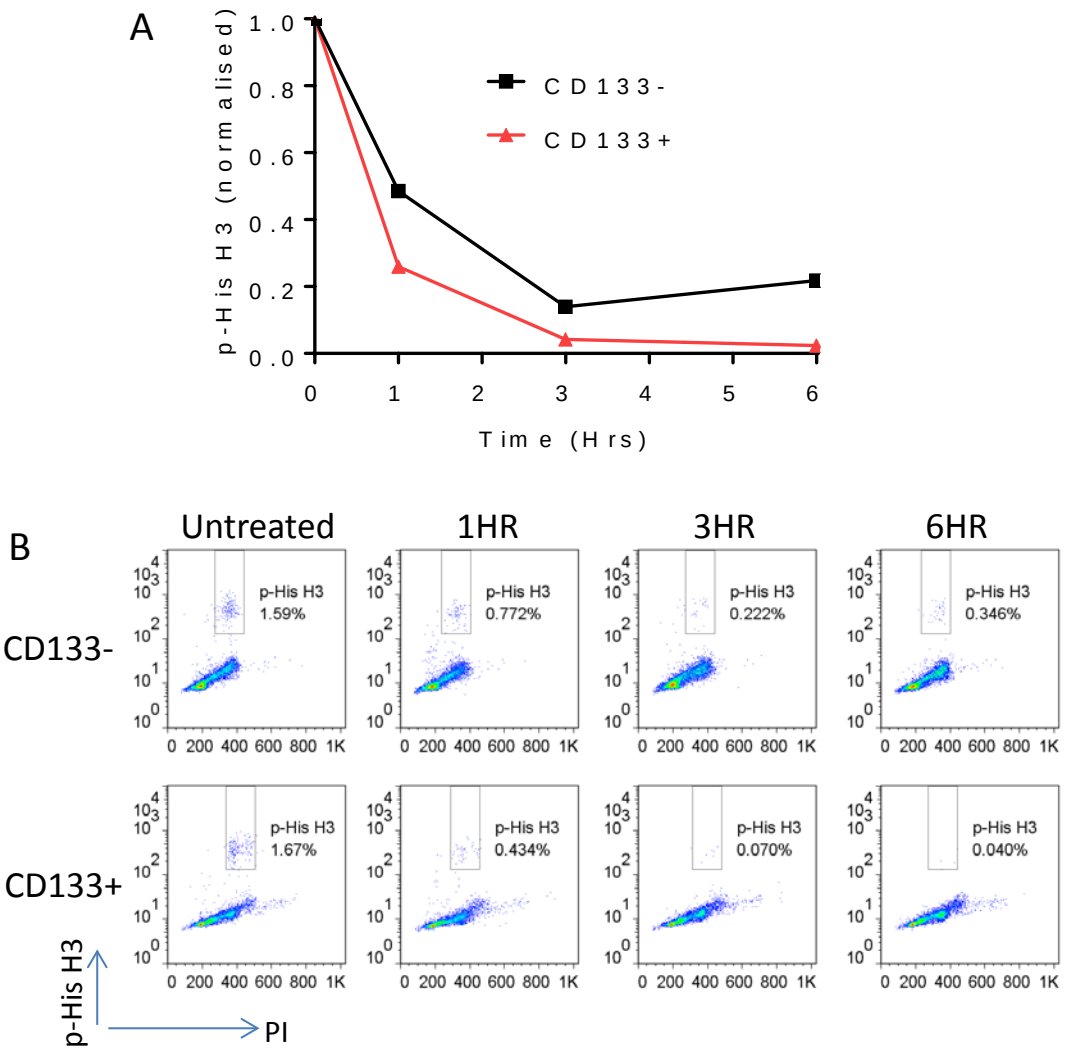

Supplementary Figure S7. Rapid activation of G2/M cell cycle checkpoint in E2 CD133+ cells CD133+ and CD133- sorted cells were irradiated with 5Gy IR followed by flow cytometry analysis of mitotic p-His H3 S10 population at the time point indicated. (**A)** Normalised data relative to untreated **(B)** representative flow cytometry profiles.

Supplementary Figure S8

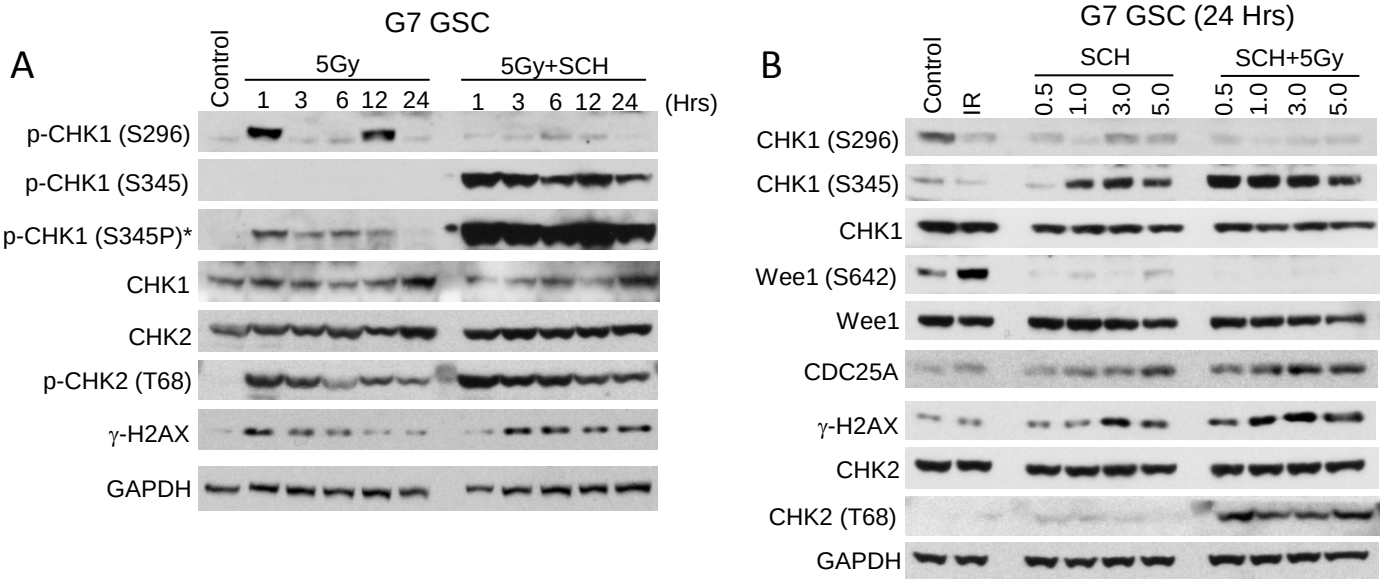

Supplementary Figure S8. Treatment of G7 GSCs with the CHK1 inhibitor SCH 900776 (SCH)
(A) Time course showing abrogation of IR induced CHK1 activation by pre-treatment of G7 GSCs with 3μM of SCH for 1hr (* denotes longer exposure). **(B)** Analysis of multiple biomarkers of CHK1 inhibition at 24 hours in G7 GSCs treated with various concentrations of SCH for 1hr followed by 5Gy IR.

Supplementary Figure S9

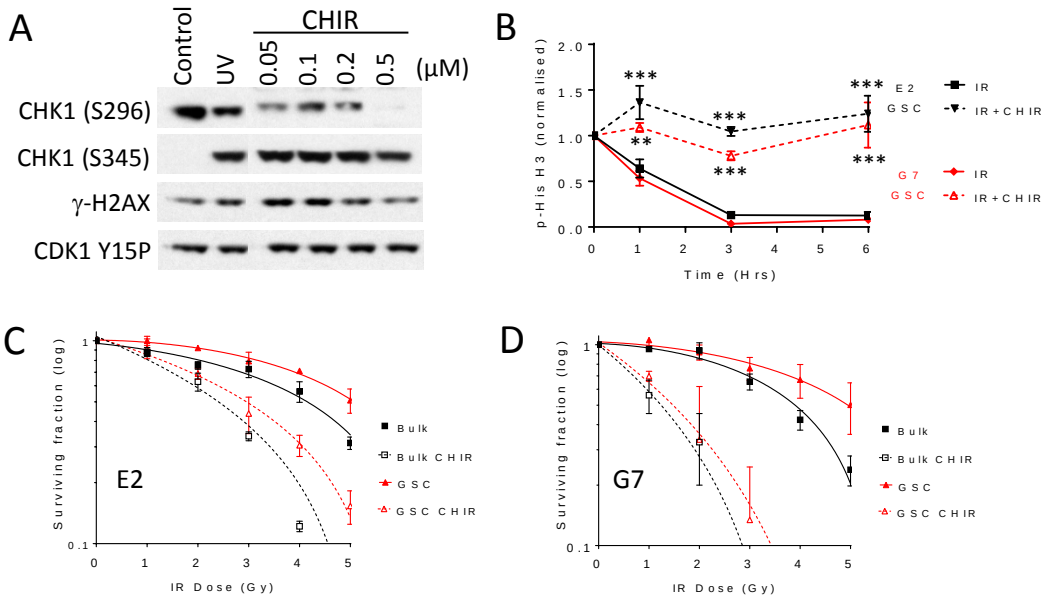

Supplementary Figure S9. Radiosensitisation of E2 and G7 cells with the CHK1 inhibitor CHIR 124 (CHIR)

(A) Dose response of CHK1 inhibition in E2 GSCs following 1 hr pre-treatment with CHIR followed by 120Jcm^{-2} UV for 1hr. **(B)** Plot summarising flow cytometry data showing inhibition of IR induced G2/M checkpoint activation in E2 and G7 GSCs treated with 0.3μM CHIR for 1hr followed by 5Gy IR, mean ± SEM from n≥3 experiments, **p<0.01,***p<0.001 relative to IR alone. **(C-D)** Clonogenic survival curves showing radiosensitisation of E2 and G7 GSCs and bulk populations following 0.3μM of CHIR treatment.

Supplementary Figure S10

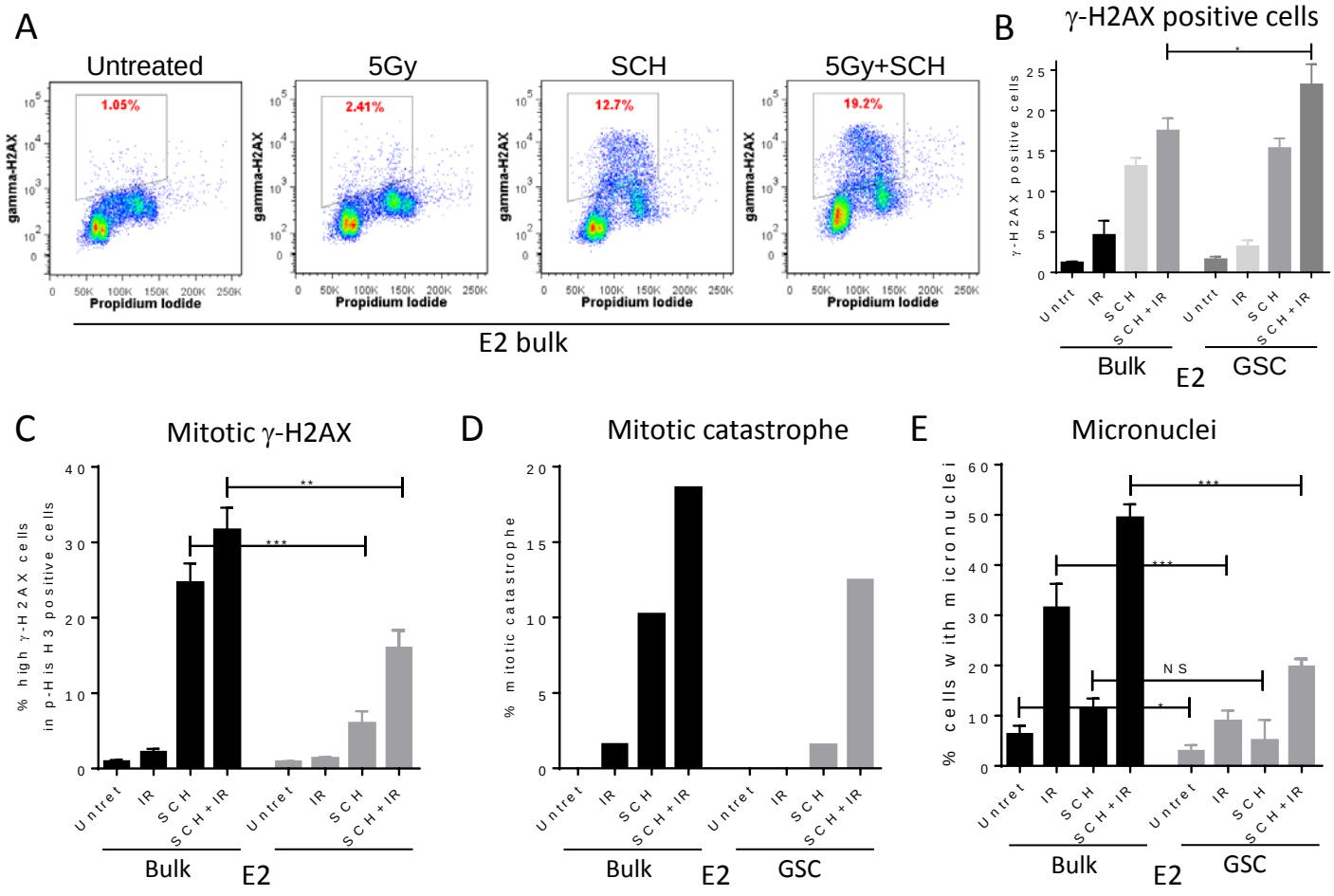

Supplementary Figure S10. Enhanced DNA repair attenuates radiosensitisation of E2 GSCs to CHK1 inhibitor (SCH)

(A) Representative flow cytometry profile of E2 bulk cells showing percentage of γ-H2AX positive cells following treatment with IR and/or CHK1 inhibitor (SCH) for 24 hours. Corresponding plots in E2 GSCs is shown in Figure 5A. **(B)** Summary of γ-H2AX data in paired bulk and stem populations, error bars show mean + SEM from 3 independent experiments, *p<0.05. **(C)** Percentage of cells with mitotic γ-H2AX, **(D)** mitotic catastrophe and **(E)** percentage of cells with micronuclei following treatment of GSC and bulk populations with IR and SCH, mean + SEM shown from three independent experiments, *p<0.05, **p<0.01,***p<0.001.

Supplementary Figure S11

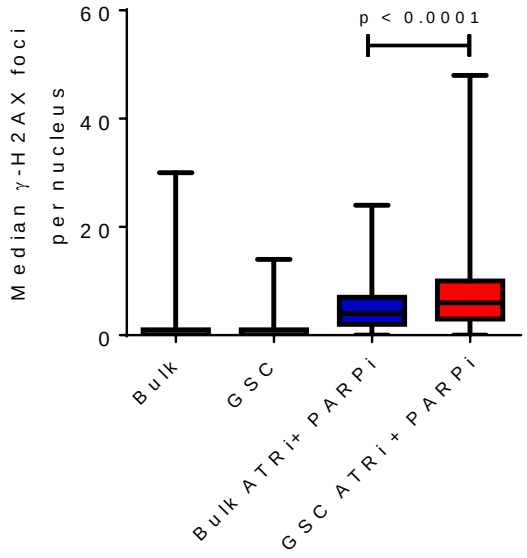

Supplementary Figure S11. Increase in γ-H2AX foci in GSCs compared to bulk population following combined ATR and PARP inhibition
Plot showing median γ-H2AX foci per nucleus in E2 bulk and GSCs following combined ATR and PARP1 inhibition at 48 hours.

Supplementary materials and methods

Maintenance of cell lines and orthotopic tumours generation

Each GBM cell line was cultured in pairs either on Matrigel ™ (Life Technology) coated flasks in AdvDMEM F12 medium (Gibco) supplemented with 1% B27 (Invitrogen), 0.5% N2 (Invitrogen), 4µg/ml heparin, 20ng/ml bFG, 20ng/ml EGF (Sigma), and 1% L-Glutamine to maintain the GSC population or in MEM (Gibco) supplemented with 10% FBS Sigma, 1% L-glutamine and 1% sodium pyruvate to deplete the GSCs and generate a differentiated tumour bulk population. All cell cultures were maintained at 37^0C, 5% CO_2. Cell lines were utilised between 6-15 passages and then discarded.

E2 GSC produced highly infiltrative tumours that resemble gliomatosis cerebri and tumour burden was significantly greater than those generated with the bulk cells. G7 GSC tumours recapitulated key histological features of GBM and demonstrated an invasive phenotype whereas tumour from the paired bulk population produced well-demarcated, non-invasive tumours.

Immunohistochemistry

Immunohistochemistry was performed on 4µm sections cut from paraffin embedded samples. Heat-mediated antigen retrieval was conducted using a pressure cooker in a microwave with sections submersed in either 10mM sodium citrate target retrieval solution pH6 (Dako, S236984) for PARP1 staining, or pH9 (Dako, S2367) for pATM staining. After blocking endogenous peroxidase (Dako, K400611-2), sections were washed in TBS-T, and PARP1 (Santa Cruz, sc8007) or pATM (S1981) (Abcam, ab81292) primary antibody was applied at an optimised dilution (1/600 PARP1, 1/200 pATM). Sections were incubated in primary antibodies overnight in a humidified chamber. The following day, sections were washed in TBS-T and secondary antibodies applied for 45mins at room temperature (Dako, K400611-2). Staining was visualised by application of 3, 3'-diaminobenzidine tetrahydrochloride (Dako, K400611-2).

Neurosphere assay

For neurosphere assay 10 GSCs were seeded into each well of a 96 well plate in 100µL medium containing the drug or relative DMSO control for 1 hour followed by mock or 2Gy irradiation. 48 hours later a further 150 µL of fresh media was added per well. Neurospheres were manually counted under 5x magnification after 3 or 4 weeks for G7 and E2 GSC respectively.

Immunofluorescence

Cells were fixed in 4% formaldehyde/PBS and permeabilised, blocked with 5% FCS, 0.5% BSA in 0.1% Triton-PBS and incubated with γ-H2AX (Millipore, 1:100) and CENPF (Abcam, 1:250) or p-His H3 S10 (Cell signalling, 1:100) antibodies overnight at 4^oC followed by incubation with appropriate Alexa Fluor 568 or 488 secondary antibodies (Invitrogen). Nuclei were counterstained with Vectashield containing DAPI (Vector laboratories). 30 Z-stack images were acquired under each condition at 63x magnification using the Zeiss LSM 710 confocal microscope analysed using Velocity software (PerkinElmer). CENPF staining was determined by the operator and pan nuclear γ-H2AX staining was excluded from the

analysis. The number of nuclei analysed for each condition ranged from 65 to 307 (CENPF positive) and 300 to 460 (CENPF negative).

Cell proliferation

200-400 cells were seeded in 96 well plates in replicates of 5. Every 24-48 hours plates were fixed in 4% formaldehyde followed by DAPI staining. Nuclei were counted using Operetta (PerkinElmer). Cell doubling times were calculated from exponential growth curve fits using GraphPad Prism.

Western blotting

Primary antibodies used for western blotting: p-CHK1 S344 (#2341), p-CHK1 S296 (#2349), CHK1 (#2345), p-ATR S428 (#2853), CHK2 (#3440S), p-CHK2 T68 (#2661), Mre11 (#4847), p-Mre11 S676 (#4859), Rad50 (#3427), NBS (#3002), p-NBS S343 (#3001), CDK1 (#9112), CDK1 Y15 (#9111), Wee1 (#4936), p-Wee1 S642 (#4910), p-CDC25C T48 (#9527), all from Cell signalling; CDC25A (ab75743), ATM (ab2618), Nestin (ab22035), SOX2 (ab75485), all from Abcam; ATR (sc1887), PARP1 (sc8007), GAPDH (sc25778), all from Santa crud; p-ATM S1981 (100-307) from Novus; CD133 (W6B3C1) from Miltenyi; γ-H2AX (JBW301) from Millipore; Olig2 (AF2418) from R&D systems and Actin (AC40) from Sigma.

Flow cytometry and cell death

For analysis of mitotic population, cells were treated and fixed with 70% ethanol and incubated with anti-phosphorylated Histone H3 serine 10 Alexa Fluor 488 conjugate antibody (1:50; Cell Signalling) for 30 minutes followed by γ-H2AX Alexa 647 antibody (1:50; Cell Signalling) for 30 minutes at room temperature. Cells were subsequently pelleted and resuspended in 1mg/ml propidium iodide (PI) containing RNAase A. Dead cells and debris were gated out using FSC and SSC and doublets decimated using PI-area vs PI-width. γ-H2AX in mitotic cells was determined by gating on the mitotic population and presenting these events on a histogram plot. Analysis of GSC markers CD133-PE (clone: 293C3) and CD15-APC (clone: VIMC6) was carried out according to manufactory instructions (Miltenyi biotech). Flow cytometry was carried out using a FACScalibur or FACSVerse.